Acta Pharmaceutica Sinica B 2022;12(7):3085–3102

Chinese Pharmaceutical Association
Institute of Materia Medica, Chinese Academy of Medical Sciences

Acta Pharmaceutica Sinica B

www.elsevier.com/locate/apsb
www.sciencedirect.com

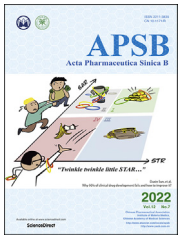

ORIGINAL ARTICLE

# Repurposing econazole as a pharmacological autophagy inhibitor to treat pancreatic ductal adenocarcinoma

**Ningna Weng[a,†], Siyuan Qin[b,†], Jiayang Liu[b], Xing Huang[c], Jingwen Jiang[b], Li Zhou[b], Zhe Zhang[b], Na Xie[b], Kui Wang[b], Ping Jin[b], Maochao Luo[b], Liyuan Peng[b], Edouard C. Nice[d], Ajay Goel[e], Suxia Han[f,*], Canhua Huang[b,*], Qing Zhu[a,*]**

[a]*Department of Abdominal Oncology, West China Hospital of Sichuan University, Chengdu 610041, China*
[b]*State Key Laboratory of Biotherapy and Cancer Center, West China Hospital, West China School of Basic Medical Sciences & Forensic Medicine, Sichuan University, Collaborative Innovation Center for Biotherapy, Chengdu 610041, China*
[c]*Department of Pancreatic Surgery, West China Hospital of Sichuan University, Chengdu 610041, China*
[d]*Department of Biochemistry and Molecular Biology, Monash University, Clayton, VIC 3800, Australia*
[e]*Department of Molecular Diagnostics and Experimental Therapeutics, Beckman Research Institute of City of Hope, Biomedical Research Center, Monrovia, CA 91016, USA*
[f]*Department of Oncology, the First Affiliated Hospital, Xi'an Jiaotong University, Xi'an 710061, China*

Received 10 October 2021; received in revised form 18 December 2021; accepted 20 December 2021

**KEY WORDS**

Econazole;
Autophagy;
PDAC;
ATF3;
AKT;
Organoid;
Trametinib;
Therapy

**Abstract** Pancreatic ductal adenocarcinoma (PDAC) is characterized by the highest mortality among carcinomas. The pathogenesis of PDAC requires elevated autophagy, inhibition of which using hydroxychloroquine has shown promise. However, current realization is impeded by its suboptimal use and unpredictable toxicity. Attempts to identify novel autophagy-modulating agents from already approved drugs offer a rapid and accessible approach. Here, using a patient-derived organoid model, we performed a comparative analysis of therapeutic responses among various antimalarial/fungal/parasitic/viral agents, through which econazole (ECON), an antifungal compound, emerged as the top candidate. Further testing in cell-line and xenograft models of PDAC validated this activity, which occurred as a direct consequence of dysfunctional autophagy. More specifically, ECON boosted autophagy initiation but blocked lysosome

*Corresponding authors.
E-mail addresses: zhuqing197202@163.com, newzhuqing1972@yahoo.com (Qing Zhu), hcanhua@hotmail.com (Canhua Huang), shan87@xjtu.edu.cn (Suxia Han).
[†]These authors made equal contributions to this work.
Peer review under responsibility of Chinese Pharmaceutical Association and Institute of Materia Medica, Chinese Academy of Medical Sciences.

https://doi.org/10.1016/j.apsb.2022.01.018

biogenesis. RNA sequencing analysis revealed that this autophagic induction was largely attributed to the altered expression of activation transcription factor 3 (ATF3). Increased nuclear import of ATF3 and its transcriptional repression of inhibitor of differentiation-1 (ID-1) led to inactivation of the AKT/mammalian target of rapamycin (mTOR) pathway, thus giving rise to autophagosome accumulation in PDAC cells. The magnitude of the increase in autophagosomes was sufficient to elicit ER stress-mediated apoptosis. Furthermore, ECON, as an autophagy inhibitor, exhibited synergistic effects with trametinib on PDAC. This study provides direct preclinical and experimental evidence for the therapeutic efficacy of ECON in PDAC treatment and reveals a mechanism whereby ECON inhibits PDAC growth.



## 1. Introduction

Pancreatic ductal adenocarcinoma (PDAC), a devastating malignancy with the highest case fatality rate among solid tumors[1,2], is characterized by near-universal activation of oncogenic *KRAS* to maintain disease progression—from premalignant lesions to advanced-stage carcinoma[1]. In addition to being typically driven by *KRAS* mutation, numerous studies have demonstrated that the pathogenesis of PDAC also relies heavily on elevated levels of autophagy—an evolutionarily conserved, self-degradative process for boosting cellular energy supplies, whereby *KRAS*-mutant PDAC cells can survive and thrive under environmental stressors, especially low-nutrient conditions[3,4].

In an effort to transform such a dependence of autophagy to specific vulnerability that can be hijacked, not surprisingly, compounds that inactivate this process have already entered clinical trials (NCT01273805, NCT01506973 and NCT03344172), as exemplified by chloroquine (CQ) and its derivative hydroxychloroquine (HCQ). However, the extent to which pharmacologic disruption of autophagy by HCQ/CQ contributes to the anti-PDAC effects is largely determined by which treatment strategy is adopted (as a monotherapy or a combination partner; NCT01506973)[5]. Another unresolved issue relates to tissue sequestration and the consequent sudden surge of CQ concentration in plasma following chronic exposure, leading to unpredictable toxicity[6]. Given the drawbacks reported for HCQ/CQ, there is an urgent need to establish a more practical treatment strategy for PDAC. Compared to the development of entirely new drugs, scouting for autophagy-modulating drugs from the neglected "arsenal" of already approved, derisked, nonantitumor agents offers an expedient shortcut with an easier clinical realization and lower overheads in terms of efficacy and safety[7–9].

Existing data using this strategy of drug repurposing have provided solid evidence for the feasibility of a shifting paradigm in drug management from development to replacement[7]. Intriguingly, the introduction of HCQ/CQ-based therapy—a proven remedy against malaria[10]—into PDAC treatment, *per se*, represents an exemplary embodiment of drug repurposing. Implicit in this paradigm is the hypothesis that better alternatives than HCQ/CQ might be approached in a similar way. Indeed, this hypothesis of developing repurposing agents to treat malarial/fungal/parasitic/viral infections for alleviating symptoms associated with multiple, if not all, cancers has been supported by the demonstration that additional therapeutic benefits, beyond their original roles, can be achieved experimentally or even clinically, *e.g.*, repurposing ketoconazole/itraconazole into prostate carcinoma treatment[11,12].

Encouraged by these alternative modes of action, an unbiased, patient-derived organoid (PDO)-based, comparative analysis of therapeutic responses among various antimalarial/fungal/parasitic/viral agents was performed, in which econazole (ECON), a broad-spectrum, antifungal compound[13], emerged as a candidate, as it exhibited more robust anti-PDAC activity than other drugs tested, including HCQ. This antitumor activity echoes previous studies in several other cancers. In some instances, the involvement of specific mechanisms leading to apoptosis has been proposed[14,15]. However, the precise mechanisms underlying the cytotoxicity of ECON on PDAC, *e.g.*, whether autophagic and apoptotic responses occur in a parallel or sequential manner, remain uncertain. Importantly, the aforementioned findings raise the possibility of its immediate, routine application in a clinical setting. However, to support this, additional *in vitro* and *in vivo* experiments are required to further validate the antitumor effect, determine rational utilization, and investigate the molecular mechanisms of ECON in PDAC treatment, paving the way for its translation from a theoretical possibility to clinical feasibility.

Herein, we demonstrate that ECON shows potent anti-PDAC activity by inducing lethal autophagy arrest both in PDO and cell line models, largely mediated by the expression of activating transcription factor 3 (ATF3). Increased nuclear expression of ATF3 and its subsequent transcriptional suppression of inhibitor of differentiation-1 (ID-1) led to inactivation of the AKT/mammalian target of rapamycin (mTOR) pathway, giving rise to autophagosome accumulation within PDAC cells under ECON exposure. The magnitude of this increase in autophagosomes is sufficient to induce endoplasmic reticulum (ER) stress-mediated apoptosis, further reinforcing the cytotoxicity of ECON in PDAC cells. Collectively, our findings provide direct preclinical and experimental evidence for the therapeutic effects of ECON against PDAC, implying a potential therapeutic opportunity with translational significance in clinical practice.

## 2. Materials and methods

### 2.1. Human specimens

Tissue specimens of PDAC were acquired from three patients undergoing surgical resection at the West China Hospital of Sichuan University (Chengdu, China). All experiments using these specimens were approved by the ethics committee (ChiCTR2100047942) and performed strictly abiding by relevant regulations of the Declaration of Helsinki under the prerequisite of

obtaining written informed consent. All samples were identified as tumor (including histopathologic type and stage) or normal tissues depending on pathologist assessment.

### 2.2. Patient-derived organoid culture

Each patient tissue was processed to establish PDO according to a set of well-established protocols[16,17]. In brief, fresh resection specimens of PDAC were minced into small fragments ($< 2$ mm$^3$) for the ease of digestion by collagenase II (5 mg/mL, Gibco) and TrypLE Express Enzyme (1 ×, Gibco) with gentle agitation at 37 °C. Following digestion, the cells were embedded in Matrigel (BD) and cultured in human complete feeding medium [advanced DMEM (AdDMEM)/F12 medium supplemented with HEPES (1%, 10 mmol/L), 1 × Glutamax, A83-01 (0.5 μmol/L), penicillin/streptomycin (1 × final concentration), B27 supplement (1 × final concentration), Primocin (50 μg/mL), mNoggin (100 ng/mL), *N*-acetyl-L-cysteine (NAC, 1.25 mmol/L), afamin/Wnt3a-conditioned medium (50% final volume), RSPO1-conditioned medium (10% final volume), hEGF (0.05 mg/mL), hGastrin I (0.01 μmol/L), hFGF10 (0.1 μg/mL), and nicotinamide (10 mmol/L)] at 37 °C in a humidified atmosphere with 5% (*v*/*v*) $CO_2$.

### 2.3. Organoid response assessment

Patient-derived PDAC organoids were dissociated into single cells, and 400 viable cells per well were plated in 384-well plates in 30 μL of 10% Matrigel in human complete medium. Drug candidates (various antimalarial/fungal/parasitic/viral agents, HCQ, trametinib or DMSO) were added, as needed, following the appearance of visibly regenerated PDAC organoids under the microscope. The therapeutic responses of organoids were monitored by observing morphological changes using time−serial optical imaging every 24 h and measured by calculating dimensional variations using Image-Pro Plus. After a 3-day exposure, the number of viable (metabolically active) cells in 3D organoids was detected using CellTiter-Glo Luminescent Assay (Promega) following the instructions of the manufacturer.

### 2.4. Cell culture

The pancreatic cancer cell lines PANC-1, AsPC-1, BxPC-3 and MIA PaCa-2 were kindly provided by Stem Cell Bank, Chinese Academy of Sciences. These cell lines were maintained in DMEM or RPMI-1640 medium supplemented with 10% fetal bovine serum, 2 mmol/L glutamine, 100 U/mL penicillin and 100 mg/mL streptomycin in a 5% $CO_2$ atmosphere at 37 °C. All cell lines used in this experiment were cultured for less than 2 months before reinitiating from authentic stocks and were routinely inspected by microscopic morphological observation and mycoplasma contamination.

### 2.5. Reagents, antibodies and plasmids

ECON, trametinib, chloroquine (CQ) and hydroxychloroquine (HCQ) were purchased from Selleck Chemicals. 3-Methyladenine (3-MA) and bafilomycin A1 (Baf-A1) were purchased from MedChem Express. Lipofectamine 3000 reagent and DAPI were purchased from Invitrogen. The plasmids were purchased from Era Biotech. Primary antibodies against cleaved caspase3, caspase3, Bcl-2, Beclin1, ATG5, AKT, p-AKT, mTOR, p-mTOR, P70S6K and p-P70S6K were acquired from Cell Signaling Technology. PARP, cleaved PARP, CK7, CK19 and Ki67 were purchased from Abcam, and LC3 and ATF3 were purchased from Novus. P62 and β-actin were obtained from Santa Cruz Biotechnology.

### 2.6. MTT assay

The short-term effect on cell growth was detected by using the 3-(4,5-dimethylthiazol-2-yl)-2,5-diphenyltetrazolium bromide (MTT) assay. Briefly, cells (2500/well) were seeded in 96-well plates. After 24 h, the cells were treated with the indicated concentrations of chemical agents for another 24 h. The detailed procedure was performed as previously described[18].

### 2.7. Colony formation assay

The long-term effect on cell growth was determined by plate colony formation assay. Cells (1000/well) were plated in 12-well plates and treated with the indicated concentration of ECON. The medium was changed every 3 days. After 1 week, the colonies were fixed with 4% paraformaldehyde for 2 h and stained with crystal violet for 30 min. Thereafter, the cells were washed three times and diluted with 0.1% SDS. Absorbance was measured at 570 nm. The soft-agar colony formation assay was performed in 6-well plates ($5 \times 10^3$/well). Cells were mixed with 0.7% agar and DMEM on a 1.2% agar underlayer. After being subjected to ECON for a week, the cells were observed by a microscope (OLYMPUS IX81).

### 2.8. Immunoblotting

Cells were seeded in six-well plates at $2 \times 10^5$ cells/well. Upon treatment, cells were harvested and digested in RIPA buffer in the presence of 1% protease inhibitor cocktail. The concentration of protein lysates was quantified using a bicinchoninic acid protein assay kit. Proteins were separated by SDS−PAGE and transferred to a PVDF membrane. After blocking in 5% skimmed milk for 90 min, the samples were incubated in suitable primary antibody at 4 °C overnight and the secondary antibody at room temperature for 90 min. Immunoreactive bands were detected by enhanced chemiluminescence reagent, with β-actin as the internal control.

### 2.9. Immunofluorescence

Cells were seeded on glass coverslips in 24-well plates at a density of $2 \times 10^4$ cells/well. After treatments, the cells were fixed in 4% formaldehyde for 2 h, permeabilized with 0.5% Triton X-100 for 20 min and blocked with 5% bovine serum albumin for 30 min. Next, the cells were incubated with primary antibodies at a dilution of 1:200 and Alexa Flour secondary antibodies. Subsequently, nuclei were stained with DAPI (1:5000) for 10 min. Cells were observed using confocal laser scanning microscopy (Zeiss, LSM 880).

### 2.10. LDH release assay

The LDH release assay was performed in 96-well plates ($5 \times 10^3$ per well) using a lactate dehydrogenase release kit (Beyotime Biotechnology, C0017). Different concentrations of ECON were added to the plates with serum-free medium. After 24 h of incubation, 80 μL of supernatant from each well was added to 40 μL

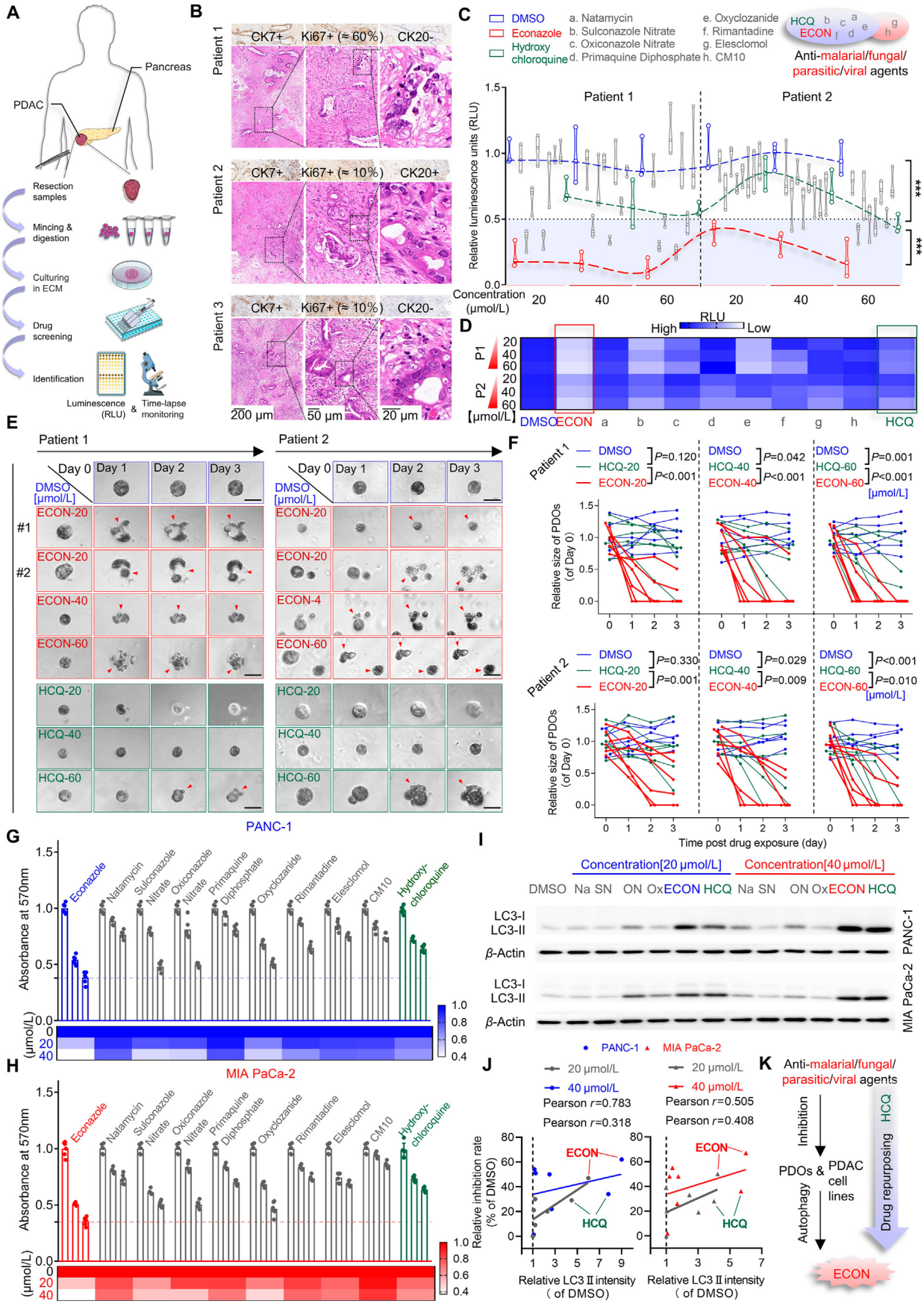
A
Pancreas
PDAC
Resection samples
Mincing & digestion
Culturing in ECM
Drug screening
Identification
Luminescence (RLU)
&
Time-lapse monitoring
B
Patient 1
Patient 2
Patient 3
CK7+
Ki67+ (≈ 60%)
Ki67+ (≈ 10%)
CK20-
CK20+
200 μm
50 μm
20 μm
C
DMSO
Econazole
Hydroxy chloroquine
a. Natamycin
b. Sulconazole Nitrate
c. Oxiconazole Nitrate
d. Primaquine Diphosphate
e. Oxyclozanide
f. Rimantadine
g. Elesclomol
h. CM10
HCQ
ECON
Anti-malarial/fungal/ parasitic/viral agents
Patient 1
Patient 2
Relative luminescence units (RLU)
Concentration (μmol/L)
***
***
D
RLU
High
Low
P1
P2
【μmol/L】
DMSO
ECON
HCQ
E
Patient 1
Patient 2
Day 0
Day 1
Day 2
Day 3
DMSO [μmol/L]
#1
#2
ECON-20
ECON-40
ECON-60
ECON-4
HCQ-20
HCQ-40
HCQ-60
PANC-1
F
Patient 1
Patient 2
DMSO
HCQ-20
ECON-20
HCQ-40
ECON-40
HCQ-60
ECON-60
P=0.120
P<0.001
P=0.042
P<0.001
P=0.001
P<0.001
[μmol/L]
P=0.330
P=0.001
P=0.029
P=0.009
P<0.001
P=0.010
Relative size of PDOs (of Day 0)
Time post drug exposure (day)
G
Absorbance at 570nm
Econazole
Natamycin
Sulconazole Nitrate
Oxiconazole Nitrate
Primaquine Diphosphate
Oxyclozanide
Rimantadine
Elesclomol
CM10
Hydroxy-chloroquine
(μmol/L)
H
MIA PaCa-2
I
Concentration[20 μmol/L]
Concentration[40 μmol/L]
DMSO
Na SN
ON
OxECON
HCQ
LC3-I
LC3-II
β-Actin
PANC-1
MIA PaCa-2
J
PANC-1
MIA PaCa-2
20 μmol/L
40 μmol/L
Pearson r=0.783
Pearson r=0.318
Pearson r=0.505
Pearson r=0.408
ECON
HCQ
Relative inhibition rate (% of DMSO)
Relative LC3 Ⅱ intensity (of DMSO)
K
Anti-malarial/fungal/ parasitic/viral agents
Inhibition
PDOs & cell lines
PDAC
Autophagy
Drug repurposing
HCQ
ECON

of LDH release reagent, and then the mixture was incubated at 37 °C for 1 h. Absorbance at 570 nm was measured with a microplate reader (MD, SpectraMax 190).

### 2.11. EdU incorporation assay

The EdU assay was performed according to the manufacturer's protocol. Following the treatments, the cells were stained with 50 mmol/L 5-ethynyl-20-deoxyuridine for 2 h at 37 °C. After fixation in 4% paraformaldehyde and permeabilization with 1% Triton X-100, the cells were stained with 1 × Apollo reaction cocktail for 30 min followed by Hoechst 33342 for another 30 min. The Hoechst-positive cells and EdU-positive cells were then immediately analyzed using an inverted fluorescence microscope (OLYMPUS IX81).

### 2.12. RNA sequencing

Cells were seeded in six-well plates at $3 \times 10^5$ cells/well. Total RNA from PANC-1 and MIA PaCa-2 cells was extracted using TRIzol reagent (Takara, China) after ECON treatment according to the manufacturer's instructions. RNA sequencing (RNA-seq) was performed on RNA prepared from two PDAC cell lines (PANC-1 and MIA PaCa-2) incubated with or without ECON. RNA-seq data generated by the Illumina HiSeq platform were aligned using TopHat (v2.0.4) with default settings (hg19) and then assembled into transcripts using Cuinks (v2.2.1), followed by quantification of gene-transcript expression profiles. To filter out genes differentially expressed in response to ECON, analysis of differentially expressed genes (DEGs) between groups (DMSO *vs*. ECON) was conducted using DESeq2 (Version 1.24.0), and statistical significance was determined by ANOVA ($\log_2$ FC [fold change] $> \pm 1$ and $P < 0.05$). By applying the DAVID database (http://www.david.niaid.nih.gov), KEGG enrichment analysis was further applied to annotate the main functions of the DEGs. TRRUST, a prediction tool of key transcription factors (http://www.grnpedia.org/trrust/), was employed to identify candidate drivers likely to regulate the enriched KEGG pathways.

### 2.13. Xenograft experiments

All experiments herein were approved by the Institutional Animal Care and Treatment Committee of Sichuan University (Chengdu, China). The animal experiments were in accordance with the NIH Guide for the Care and Use of Laboratory Animals. Xenograft models were established in 6-week-old male BALB/c nude mice purchased from Beijing HFK Bioscience. PANC-1 cells ($1 \times 10^7$ cells/mouse) were subcutaneously injected into the right flanks of the nude mice. After ~2 weeks, when the tumor volume reached ~100 $mm^3$, the mice were randomly divided into different groups. In Fig. 2E, group 1 received 100 μL of vehicle, and group 2 received 50 mg/kg ECON. Vehicle or ECON was injected intraperitoneally daily for 2 weeks. In Fig. 7G, when the tumor volumes reached ~100 $mm^3$, mice bearing PDAC xenografts were randomly divided into 6 groups and received the following treatments: i) vehicle; ii) 25 mg/kg ECON; iii) 25 mg/kg CQ; iv) 1 mg/kg trametinib; v) 25 mg/kg ECON+1 mg/kg trametinib; and vi) 25 mg/kg CQ+1 mg/kg trametinib. The mouse weight and tumor volume were monitored every 2 days once the tumor became palpable. The mice were sacrificed at 2 weeks post-treatment, and tumor tissues were isolated and prepared for further analysis.

### 2.14. Immunohistochemistry

The tumor samples and the main heart, liver, spleen, lung and kidneys removed from xenograft models were embedded in paraffin wax and cut into 4 μm sections. The sections were dewaxed and rehydrated, and endogenous peroxidase activity was quenched before treatment with citrate buffer for antigen retrieval. After incubation with the indicated primary antibodies at 4 °C overnight, the sections were stained with diaminobenzidine and counterstained with Mayer hematoxylin. The sections were stained with H&E. Imaging was visualized with a DM2500 fluorescence microscope.

### 2.15. RNA interference

The scrambled siRNAs were custom synthesized chemically by GenePharma and resuspended according to the manufacturer's instructions. The cells were transfected at approximately 40% confluency using Lipofectamine 3000 reagent. Experiments were performed 48 h after transfection, and the siRNA effect was verified by immunoblotting analysis. The sequences of the siRNAs involved are listed in Table S1.

### 2.16. Immunoprecipitation

After designated treatments, cells were collected and solubilized in RIPA buffer containing 1% protease inhibitors. Next, the cell lysates were incubated in 1 μg of antibodies and rotated at 4 °C overnight. Immunoblotting analysis was performed followed by pull down of immunoprecipitated protein with Protein A beads.

### 2.17. RNA isolation and quantitative real-time PCR

Total RNA was extracted from cells after treatment, and cDNA was synthesized using a TaKaRa PrimeScript RT reagent kit (Takara, RR014) according to the manufacturer's protocol. The expression status of the candidate genes was determined using an ABI 7900HT Real-Time PCR system (Applied Biosystems, Inc., USA). Primer sequences are listed in Supporting Information Table S2.

**Figure 1** Therapeutic responses in PDAC organoid and cell-line models. (A) Schematic overview of PDAC PDOs establishment and drug assessment. (B) H&E stain of 3 PDAC tissues for organoid development. (C) The relative luminescence unit (RLU) of organoids treated with indicated concentrations of drug candidates. (D) Quantification of (C). (E) Brightfield images of organoids treated with indicated concentrations of ECON or HCQ, scale bar: 100 μm. (F) Kill curves for organoids in (E). (G, H) MTT assay of PANC-1 and MIA PaCa-2 incubated with different agents (20 and 40 μmol/L, 24 h). (I) Immunoblot analysis of LC3 in PDAC cells treated with indicated concentrations of sulconazole nitrate, oxiconazole nitrate, oxyclozanide, ECON and hydroxychloroquine for 24 h. (J) Correlation analysis of inhibition rate and LC3-II expression in PDAC cells treated with drug candidates. (K) Schematic overview of identifying ECON. Data are presented as mean ± SD, $n = 3$; $^*P < 0.05$; $^{**}P < 0.01$, $^{***}P < 0.001$.

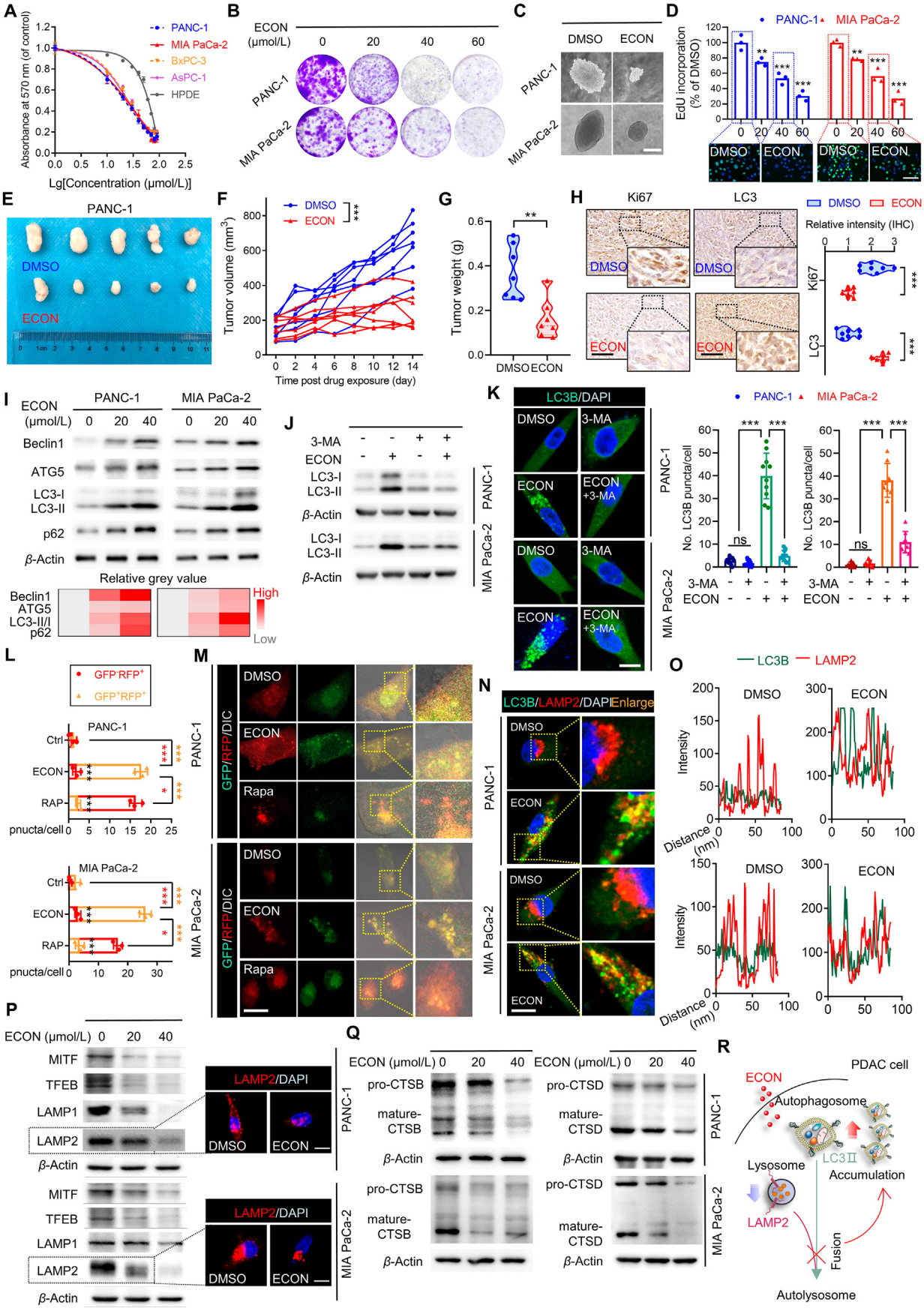
A
Absorbance at 570 nm (of control)
Lg[Concentration (μmol/L)]
PANC-1
MIA PaCa-2
BxPC-3
AsPC-1
HPDE
B
ECON (μmol/L) 0 20 40 60
PANC-1
MIA PaCa-2
C
DMSO ECON
PANC-1
MIA PaCa-2
D
PANC-1 MIA PaCa-2
EdU incorporation (% of DMSO)
DMSO ECON DMSO ECON
E
PANC-1
DMSO
ECON
F
DMSO
ECON
Tumor volume (mm3)
Time post drug exposure (day)
G
Tumor weight (g)
DMSO ECON
H
Ki67 LC3
DMSO ECON
Relative intensity (IHC)
Ki67
LC3
I
ECON (μmol/L) PANC-1 MIA PaCa-2 0 20 40 0 20 40
Beclin1
ATG5
LC3-I
LC3-II
p62
β-Actin
Relative grey value
High
Low
J
3-MA
ECON
LC3-I
LC3-II
β-Actin
PANC-1
MIA PaCa-2
K
LC3B/DAPI
DMSO 3-MA ECON ECON +3-MA
PANC-1 MIA PaCa-2
No. LC3B puncta/cell
ns
L
GFP-RFP+
GFP+RFP+
PANC-1
Ctrl
ECON
RAP
pnucta/cell
MIA PaCa-2
M
GFP/RFP/DIC
DMSO
ECON
Rapa
PANC-1
MIA PaCa-2
N
LC3B/LAMP2/DAPI Enlarge
PANC-1
MIA PaCa-2
O
LC3B LAMP2
DMSO ECON
Intensity
Distance (nm)
P
ECON (μmol/L) 0 20 40
MITF
TFEB
LAMP1
LAMP2
β-Actin
LAMP2/DAPI
DMSO ECON
Q
ECON (μmol/L) 0 20 40
pro-CTSB
mature-CTSB
pro-CTSD
mature-CTSD
β-Actin
PANC-1
MIA PaCa-2
R
PDAC cell
ECON
Autophagosome
LC3Ⅱ
Accumulation
Lysosome
LAMP2
Fusion
Autolysosome

### 2.18. Tissue microarray and PDAC tissue

A PDAC tissue microarray was purchased from Alenabio, and PDAC tissues were obtained from West China Hospital with informed consent. Tumor tissue was generated from formalin-fixed, paraffin-embedded tissues from PDAC patients. Patients were followed up regularly. The microarray clinical information is presented in Supporting Information Table S3, and PDAC patients are presented in Supporting Information Table S4. Pathological grading was measured by two independent pathologists at our center.

### 2.19. Flow cytometry

The apoptotic ratio was measured with an Annexin V−FITC/propidium iodide (PI) detection kit (KeyGEN BioTECH, KGA108). Procedures were performed according to the manufacturer's protocol. Briefly, the cells were resuspended in 500 mL binding buffer and incubated with 5 μL Annexin V−FITC and 5 μL PI for 10 min each. At least $2 \times 10^4$ live cells were analyzed on a FACSCalibur flow cytometer (BD Biosciences, San Jose, CA, USA). For the measurement of intracellular ROS levels, the cells were incubated with 10 μmol/L DCFHDA for 30 min at 37 °C before analysis. Data were analyzed by using FlowJo software.

### 2.20. Statistical analysis

Statistical analysis was performed with GraphPad Prism v8.0.1 (La Jolla, CA, USA; https://www.graphpad.com). One/two-way ANOVA or Student's *t* test was applied to determine statistical significance. All data are presented as the mean ± standard deviation (SD). $^*P < 0.05$, $^{**}P < 0.01$, and $^{***}P < 0.001$ are considered statistically significant.

## 3. Results

### 3.1. Assessment of therapeutic responses in PDAC organoid and cell line models

Given the essential functional requirement of autophagy to fuel tumorigenic growth of PDAC cells and the drawbacks reported for HCQ clinically, we performed an unbiased, comparative analysis of therapeutic responses among various anti-malarial/fungal/parasitic/viral agents to search for better alternatives. To establish clinically relevant PDAC models for predicting and testing the drug responses of individual patients *in vitro*[19], we generated three independent PDAC PDOs using freshly resected samples ranging from low- (patients 1 and 2) to high-grade invasive adenocarcinoma (patient 3) (Fig. 1A and Supporting Information Table S5). Based on the pathologist's assessment, all surgical resection specimens used for PDO generation were confirmed to be PDACs by hematoxylin and eosin (H&E) staining sections and immunohistochemical (IHC) staining with cytokeratin (CK) 7, Ki67 and CK19 (Fig. 1B and Supporting Information Fig. S1A). Among them, luminal cytokeratins CK7 and CK19 are frequently used markers of the pancreatic duct, and Ki67 is a reliable indicator of cellular proliferation in the clinic. In addition to the histopathologic diagnosis, the plain and enhanced abdominal computed tomography (CT) scan of the patients revealed poorly demarcated, cyst-like, neoplastic low-density lesions with inhomogeneous enhancement in the pancreatic tail (patients 1 and 2) or head (patient 3) (Fig. S1B). Additionally, it should be noted that our culture conditions and experimental procedures were in accordance with those previously well-described protocols for human PDAC organoids (see methods).

Using this preclinical model, we found that organoids derived from low-grade invasive PDAC patients (patients 1 and 2) showed more robust responses to the antifungal ECON than other candidates (including HCQ) by employing a CellTiter-Glo cell viability assay (Fig. 1C and D). Importantly, such differences in therapeutic potency between ECON and HCQ were particularly noticeable when low doses of drugs (20 or 40 μmol/L) were applied (Fig. 1C and D). Furthermore, as the duration of drug exposure increased, we noted that PDOs under ECON treatment exhibited dramatic morphological alterations *via* 3-day serial monitoring, which was characterized by the sharpest decline in overall size among all the candidates measured (Fig. 1E and F, Supporting Information Fig. S2A and S2B). Meanwhile, this change in ECON-treated PDOs occurred earlier than that in other groups at different concentrations ranging from 20 to 60 μmol/L, particularly the HCQ-treated PDOs (Fig. 1E, F, Fig. S2A and S2B). Similar therapeutic effects of ECON were further validated in organoids from patient 3 who suffered from high-grade invasive PDAC (Fig. S2C and S2D). Taken together, these data indicate that among all the candidates tested, ECON stands out as a more potentially effective alternative to HCQ by assessing their therapeutic responses in PDAC organoid models.

To extend and generalize these findings further, we evaluated the growth-inhibitory activity of these drug candidates in two human PDAC cell lines (PANC-1 and MIA PaCa-2). In an echo of the observation in PDAC PDOs, the cytotoxicity of ECON but not HCQ was still most pronounced in both cell lines (Fig. 1G and H), indicating that the applicable scope of ECON for PDAC might not be limited to a given patient or model.

Since our prime objective was to search for alternatives to HCQ, the above findings raised the question of whether the

**Figure 2** ECON exhibits potent anti-PDAC effects with impaired autophagic flux. (A) MTT assay of PDAC cell lines and HPDE incubated with indicated concentrations of ECON for 24 h. (B−D) Cell proliferation of PDAC cells treated with indicated concentrations of ECON was measured by plate- and soft agar colony formation (B, C) and EdU incorporation (D), scale bar: 100 μm. (E) The tumors from mice treated with ECON or vehicle. (F, G) Tumor volumes and weights in (E). (H) Immunohistochemical staining of Ki67 and LC3 in tumor tissues (scale bar: 100 μm). (I) Immunoblot analysis of LC3, Beclin1, ATG5 and p62 in ECON-treated cells with indicated concentrations for 24 h. (J) Immunoblot analysis of LC3 in cells treated with or without ECON (20 μmol/L) in the presence or absence of 3-MA (5 mmol/L, 24 h). (K) Immunofluorescence analysis of LC3 in cells treated as in (J), scale bar: 10 μm. (M) Immunofluorescence analysis of PDAC cells transiently transfected with GFP-mRFP-LC3 and treated with or without ECON (20 μmol/L, 24 h), scale bar: 10 μm. Cells incubated with rapamycin served as positive control. (L) Quantification of (M). (N) Co-localization of LC3 and LAMP2 in cells incubated with or without ECON (20 μmol/L, 24 h), scale bar: 10 μm. (O) Quantification of (N). (P) Immunoblot analysis of MITF, TFEB, LAMP1and LAMP2 in cells treated as in (I), scale bar: 10 μm. (Q) Immunoblot analysis of CTSB and CTSD in cells treated as in (I). (R) Schematic overview. Data are presented as mean ± SD, $n = 3$; $^*P < 0.05$; $^{**}P < 0.01$, $^{***}P < 0.001$, ns, no significant.

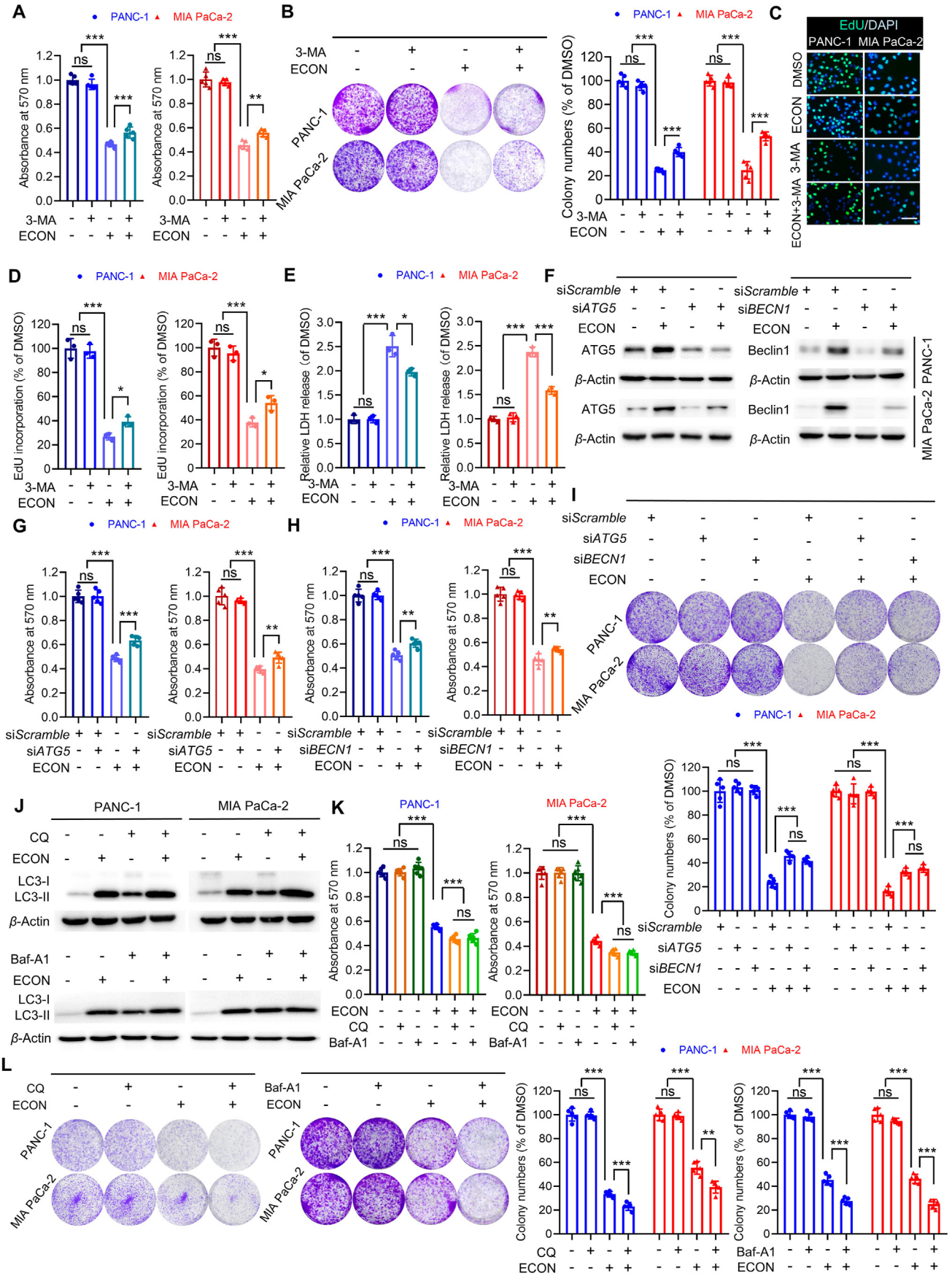
A
PANC-1 MIA PaCa-2
Absorbance at 570 nm
3-MA
ECON
B
3-MA
ECON
PANC-1
MIA PaCa-2
Colony numbers (% of DMSO)
C
EdU/DAPI
PANC-1 MIA PaCa-2
DMSO
ECON
3-MA
ECON+3-MA
D
EdU incorporation (% of DMSO)
E
Relative LDH release (of DMSO)
F
siScramble
siATG5
siBECN1
ECON
ATG5
Beclin1
β-Actin
PANC-1
MIA PaCa-2
G
H
I
J
PANC-1
MIA PaCa-2
CQ
ECON
LC3-I
LC3-II
β-Actin
Baf-A1
K
L
ns

responses of PDAC cells to different drug candidates were associated with the degree to which these antimalarial/fungal/parasitic/viral agents may impact the cellular autophagy machinery. To address this issue, we investigated the expression changes of the autophagosome marker microtubule-associated protein light chain 3 (LC3) in PDAC cells before and after 24 h in culture with different drug candidates (Fig. 1I). Supporting our hypothesis, the cytotoxic effects of such compounds against PDAC cells (PANC-1 and MIA PaCa-2) were found to correlate positively with the magnitude of increases in the conversion of the cytosolic form of LC3 (LC3-I) to the conjugate form of LC3-I with phosphatidylethanolamine (LC3-II), especially under relatively low-dose (20 μmol/L) exposure (see heavy lines in Fig. 1J for correlational analyses; $r = 0.783$ and $r = 0.522$, respectively). Intriguingly, the responses of PDAC cells to ECON did represent a typical performance of this correlation that we would expect to observe, *i.e.*, yielding potent cytotoxicity accompanied by a dramatic influence on the expression of LC3-II (Fig. 1J). Actually, this massive increase in autophagosomes induced by ECON has gone far beyond the scope of what PDAC cells could withstand, possibly moving the controlled, pro-survival autophagy into an uncontrolled, pro-death mechanism in which lysosomal scavenging pathways were blocked to varying degrees. Hence, in this regard, such responses to ECON may be conceptually similar to the way HCQ worked, but the efficacy of ECON on growth inhibioton and autophagy modulation is stronger than HCQ in PDAC (Fig. 1I and J). Together, these results demonstrate that ECON exhibits potent anti-PDAC effects, which are obviously characterized by dysregulated autophagy (Fig. 1K).

### 3.2. *ECON exhibits potent anti-PDAC effects with impaired autophagic flux*

As the novel role of ECON in treating PDAC emerged (Supporting Information Fig. S3A), it is of great importance to perform in-depth analyses of its anti-PDAC activity. Therefore, we performed an MTT assay to examine cell viability following ECON exposure in multiple human PDAC cell lines (PANC-1, MIA PaCa-2, AsPC-1 and BxPC-3), as well as an immortalized, non-tumorigenic human pancreatic duct epithelial (HPDE) cell line. Of note, when compared to HPDE [half maximal inhibitory concentration ($IC_{50}$) of 128 μmol/L], the growth of PDAC cell lines was dramatically repressed by ECON, with $IC_{50}$ values ranging from 20 to 30 μmol/L (Fig. 2A and Fig. S3B), implying a high efficiency and neoplastic-cell specificity of ECON, at least *in vitro*. Consistently, treating PDAC cells with ECON also resulted in decreased clonogenicity and proliferative capacity, demonstrated by 2D (plate)- and 3D (agarose)-colony formation and EdU incorporation assays (Fig. 2B−D and Fig. S3D). We then performed cell morphological observation and lactate dehydrogenase (LDH), and found that ECON exhibited significant cytotoxicity in PDAC cells (Fig. S3C and S3E). Furthermore, to better mimic a clinical scenario to evaluate the effectiveness and safety of ECON *in vivo*, we next established a cell line (PANC-1)-derived xenograft mouse model through subcutaneous implantation. As expected, tumour burden estimated volumetrically and gravimetrically revealed a significant growth-inhibitory effect of ECON ($P < 0.001$ and $P < 0.01$, respectively) without obvious weight loss and visceral toxicity following intraperitoneal administration for a 14-day period (Fig. 2E−G, Fig. S3F and S3G). Moreover, tissues from mice that received ECON showed a decrease in the expression of the proliferation marker Ki67 and an increase in LC3 by IHC staining, in contrast to vehicle-treated tissues (Fig. 2H). Hence, these results demonstrate that ECON exhibits strong antitumor potency against PDAC both *in vitro* and *in vivo*; this effect tends to be not followed by serious adverse reactions or even suspected toxicity, *i.e.*, the therapeutic benefits of ECON alone outweigh the risks.

Consistent with the preliminary exploration, the results of immunoblotting and immunofluorescence analyses demonstrate that PANC-1 and MIA PaCa-2 cells upon ECON treatment exhibited intense autophagic induction, as evidenced by the gradiently increased expression of LC3-II and pro-autophagic proteins [Beclin1 and autophagy-related gene 5 (ATG5)] in a dose- and time-dependent manner, together with the cytoplasm retention of characteristic autophagic vacuoles and LC3 puncta (Fig. 2I, Supporting Information Fig. S4A and S4B). In further support of an autophagy-promoting role for ECON, this induction was also validated by immunoprecipitation, which revealed a disruption of the interaction between Beclin1 and Bcl-2 in PDAC cells caused by ECON use (Fig. S4C). Being regarded as a 'rheostat' to regulate basal levels of autophagy, such dissociation of the Beclin1−Bcl-2 complex can thereby potentially free resources for the assembly of the Beclin1−VPS34 initiation complex[20,21]. Moreover, the contributions made by ECON to autophagic induction could be significantly attenuated through pharmacological inhibition using the PI3K inhibitor 3-methyladenine (3-MA) or through siRNA-mediated silencing of autophagic machinery components (*i.e.*, *ATG5* and *BECN1*) (Fig. 2J, K, and Fig. S4D−S4F). Thus, it is apparent that ECON treatment can induce excessive autophagy in PDAC cells.

To further determine whether the cytotoxic effect could be attributed to dysfunctional autophagy, we investigated autophagic flux of PDAC cells in response to ECON exposure. Indeed, ahead of immunofluorescent examinations, this idea was first suggested by the observation that the cumulative expression of p62/SQSTM1, an autophagy-specific substrate, was triggered by ECON in PDAC cells along with increased concentration and prolonged time (Fig. 2I and Fig. S4A). As predicted, an in-depth study along this line using a tandem mRFP-GFP-tagged LC3B construct identified that autophagic flux was largely blocked in ECON-treated PDAC cells, as manifested by increased autophagosomes (yellow dots, $RFP^+$ $GFP^+$) and decreased autolysosomes (red dots, $RFP^+$ $GFP^-$) when compared with those in the rapamycin-treated positive control groups (Fig. 2L and M). The possible involvement of attenuated autophagic flux was further identified by the infrequent but observable colocalization of LC3B with lysosomal associated membrane protein 2 (LAMP2) in

**Figure 3** Autophagy arrest contributes to the anti-PDAC activity of ECON. (A) MTT assay of cells incubated with or without ECON (20 μmol/L) in the presence or absence of 3-MA (5 mmol/L, 24 h). (B−E) Colony formation, EdU incorporation (scale bar: 100 μm) and LDH release assay of PDAC cells treated as in (A). (F) Immunoblot analysis of ATG5 and Beclin1 in PDAC cells transfected with si*Scramble*, si*ATG5*, or si*BECN1*, following treatment with or without ECON (20 μmol/L, 24 h). (G−I) MTT and colony formation assay treated as in (F). (J) Immunoblot analysis of LC3 in PDAC cells treated with ECON in the absence or presence of Baf-A1 (100 nmol/L) or CQ (10 μmol/L). (K, L) MTT and colony formation assay treated as in (J). Data are presented as mean ± SD, $n = 3$; *$P < 0.05$; **$P < 0.01$, ***$P < 0.001$, ns, no significant.

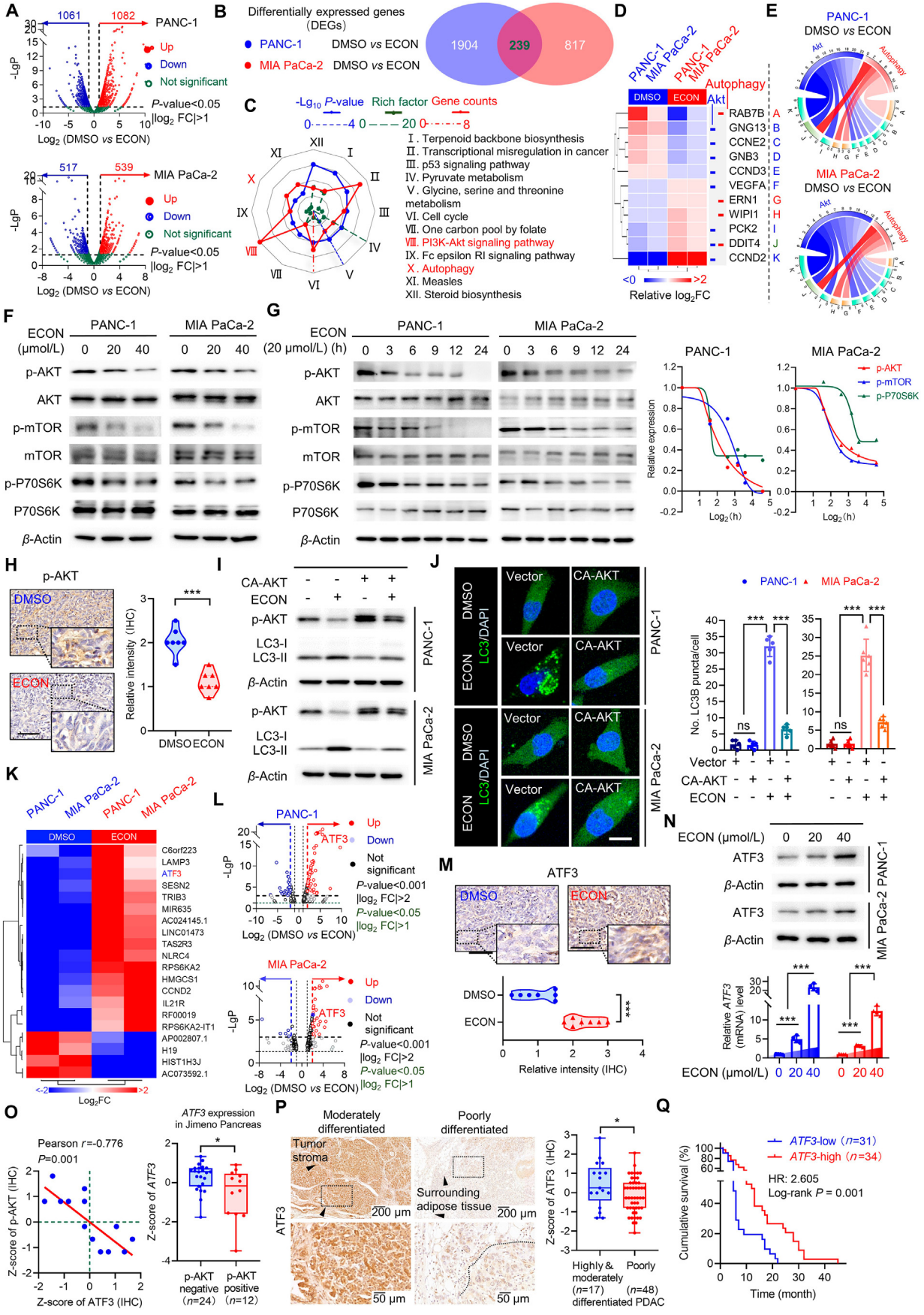
A
PANC-1
1061
1082
Up
Down
Not significant
P-value<0.05
|log2 FC|>1
Log2 (DMSO vs ECON)
MIA PaCa-2
517
539
B
Differentially expressed genes (DEGs)
PANC-1 DMSO vs ECON
MIA PaCa-2 DMSO vs ECON
1904
239
817
C
-Lg10 P-value
Rich factor
Gene counts
Ⅰ. Terpenoid backbone biosynthesis
Ⅱ. Transcriptional misregulation in cancer
Ⅲ. p53 signaling pathway
Ⅳ. Pyruvate metabolism
Ⅴ. Glycine, serine and threonine metabolism
Ⅵ. Cell cycle
Ⅶ. One carbon pool by folate
Ⅷ. PI3K-Akt signaling pathway
Ⅸ. Fc epsilon RI signaling pathway
Ⅹ. Autophagy
Ⅺ. Measles
Ⅻ. Steroid biosynthesis
D
Autophagy
DMSO
ECON
Akt
RAB7B
GNG13
CCNE2
GNB3
CCND3
VEGFA
ERN1
WIPI1
PCK2
DDIT4
CCND2
Relative log2FC
E
PANC-1
DMSO vs ECON
MIA PaCa-2
DMSO vs ECON
F
ECON (μmol/L)
PANC-1
MIA PaCa-2
p-AKT
AKT
p-mTOR
mTOR
p-P70S6K
P70S6K
β-Actin
G
ECON (20 μmol/L) (h)
PANC-1
MIA PaCa-2
Relative expression
Log2(h)
p-AKT
p-mTOR
p-P70S6K
H
p-AKT
DMSO
ECON
Relative intensity (IHC)
I
CA-AKT
ECON
p-AKT
LC3-I
LC3-II
β-Actin
PANC-1
MIA PaCa-2
J
DMSO
ECON
LC3/DAPI
Vector
CA-AKT
No. LC3B puncta/cell
ns
K
PANC-1
MIA PaCa-2
C6orf223
LAMP3
ATF3
SESN2
TRIB3
MIR635
AC024145.1
LINC01473
TAS2R3
NLRC4
RPS6KA2
HMGCS1
CCND2
IL21R
RF00019
RPS6KA2-IT1
AP002807.1
H19
HIST1H3J
AC073592.1
Log2FC
L
PANC-1
MIA PaCa-2
Up
Down
Not significant
P-value<0.001
|log2 FC|>2
P-value<0.05
|log2 FC|>1
Log2 (DMSO vs ECON)
M
ATF3
DMSO
ECON
Relative intensity (IHC)
N
ECON (μmol/L)
ATF3
β-Actin
Relative ATF3 (mRNA) level
O
Pearson r=-0.776
P=0.001
Z-score of p-AKT (IHC)
Z-score of ATF3 (IHC)
ATF3 expression in Jimeno Pancreas
Z-score of ATF3
p-AKT negative (n=24)
p-AKT positive (n=12)
P
Moderately differentiated
Poorly differentiated
Tumor stroma
Surrounding adipose tissue
200 μm
50 μm
Z-score of ATF3 (IHC)
Highly & moderately differentiated (n=17)
Poorly differentiated PDAC (n=48)
Q
ATF3-low (n=31)
ATF3-high (n=34)
HR: 2.605
Log-rank P = 0.001
Cumulative survival (%)
Time (month)

PDAC cells upon ECON treatment (Fig. 2N and O) and helped to explain why this blockage occurred. That is, the insufficient autophagic clearance induced by ECON might be explained by decreased lysosomal biogenesis rather than attributed to altered lysosomal activity.

Considering the nexus role of MiT/TFE transcription factors (TFs) in linking autophagy to lysosomal biogenesis[22,23], the question arose as to whether the rare appearance of autolysosomes induced by ECON was caused by these TFs. To resolve this question, we explored alterations in MiT/TFE factor expression, lysosome numbers [lysosome-associated membrane protein 1 (LAMP1) and lysosome-associated membrane protein 2 (LAMP2)], and lysosomal cathepsin (CTS) activity (CTSD and CTSB) in PDAC cells in response to ECON. Strikingly, the above cause−effect chain was weakened collaboratively in PDAC cells by an increase in ECON dose (0 to 40 μmol/L, Fig. 2P and Q), thus giving rise to limited autolysosome biogenesis, decreased autolysosomal degradation and enriched ubiquitin−protein conjugates (Fig. 2P, Q, Fig. S4G and S4H). This dysfunctional autophagy partially revealed the mechanisms underlying the correlation between ECON-induced cytotoxicity and autophagosome accumulation. In summary, these data underscore that ECON boosts autophagy initiation but blocks lysosome biogenesis, *i.e.*, impaired autophagic flux, in PDAC cells (Fig. 2R).

### 3.3. Autophagy arrest contributes to the anti-PDAC activity of ECON

Based on the above findings, the role of impaired autophagic flux in ECON-induced cytotoxicity has become the core issue to be solved, and inhibitors targeting different autophagic phases were therefore used. As shown in Fig. 3A, the growth of ECON-treated PDAC cells was markedly restored through inhibiting autophagy initiation with 3-MA, which was further validated by colony formation, EdU incorporation and LDH release assays (Fig. 3B−E). In addition to pharmacological inhibition, similar observations were also found by genetic silencing of key autophagy-specific genes (*ATG5* or *BECN1*, Fig. 3F−I), highlighting the necessary role of autophagic induction in ECON-triggered cytotoxicity. In contrast, when combined with CQ or bafilomycin A1 (Baf-A1, two late-autophagy inhibitors), the antitumor activity of ECON in PDAC cells was significantly exacerbated due to the substantial accumulation of autophagosomes, as demonstrated by enhanced LC3-II expression and reduced cell growth and colony-formation capacity (Fig. 3J−L). Hence, the increased accumulation of intracellular autophagosomes contributes to the anti-PDAC effect of ECON.

### 3.4. Identification of the ATF3/AKT axis involved in ECON-induced autophagy

Next, to investigate the mechanism underlying ECON-mediated autophagy, RNA sequencing (RNA-seq) was performed in two PDAC cell lines incubated with or without ECON, and 239 overlapping differentially expressed genes (DEGs) were filtered for statistical significance ($P < 0.05$, $\log_2$FC [fold change] $> \pm 1$) (Fig. 4A and B). These DEGs were grouped by Kyoto Encyclopedia of Genes and Genomes (KEGG) analysis using the DAVID bioinformatics tool, deciphering multiple putative downstream signaling pathways of ECON treatment (Fig. 4C). These included autophagy and the PI3K−AKT pathway as two enriched ECON-associated signaling cascades (Fig. 4C−E), the latter of which is a well-established pathway for regulating autophagy. Therefore, we examined whether the AKT/mTOR signaling pathway was also involved in ECON-induced autophagy initiation. As shown in Fig. 4F and G, the expression of phosphorylated AKT (p-AKT), mTOR, and P70S6K was significantly decreased in ECON-treated PDAC cells. Consistently, the downregulation of p-AKT was also observed in posttreatment (ECON) tissues by IHC staining (Fig. 4H). Along with these lines, we then transfected PDAC cells with a constitutively active form of AKT (CA-AKT) and found that counteracting ECON-induced suppression of p-AKT could strongly inhibit the conversion of LC3-I to LC3-II and LC3 puncta formation (Fig. 4I and J). Together, these results suggest that autophagic induction is driven by ECON-mediated inactivation of AKT/mTOR signaling.

Curious about how AKT/mTOR signaling was regulated during ECON exposure, we re-examined the DEGs and adopted stricter filter criteria ($P < 0.001$, $\log_2$FC [fold change] $> \pm 2$) for selecting candidate drivers, whereby 20 genes stood out (Fig. 4K). Based on the summary of enrichment analysis in TRRUST[24], we noticed ATF3 for its scoring ranked second and the most remarkable increase in mRNA level (Supporting Information Fig. S5A and S5B). Without exception, this increase was confirmed in both cultured PDAC cells and xenograft tissues (Fig. 4L−N). Consistent with a previous study supporting a role for ATF3 as a negative regulator in the AKT pathway in prostate carcinoma[25], it was found that ECON-induced ATF3 overexpression was inversely associated with the level of p-AKT by histological analyses (Fig. 4), suggesting that a pathway similar to ATF3/AKT axis might exist in PDAC. The role of ATF3 as a suppressor in PDAC was preliminary confirmed by employing the Oncomine database, tissue microarray and cell-line analysis (Fig. S5C−S5H), echoing its effect in other carcinomas[26,27]. To further explore the prognostic value of ATF3 in PDAC, we analyzed the correlation between ATF3 expression and patient

**Figure 4** Identification of ATF3/AKT axis involved in ECON-induced autophagy. (A) Volcano Plot indicated DEGs identified by RNA-seq of PDAC cells treated with or without ECON for 24 h. (B) Venn diagram showed the number of overlapped DEGs in (A). (C) Radar chart depicted 12 pathways enriched with the DEGs. (D) Heat map of DEGs in (A). (E) Chord graph indicated 11 DEGs involved in AKT pathway and autophagy pathway. (F) Immunoblot analysis of total and phosphorylated AKT, mTOR, P70S6K in cells treated with indicated concentrations of ECON for 24 h. (G) Immunoblot analysis of parent and phosphorylated AKT, mTOR, P70S6K in cells treated with 20 μmol/L ECON for indicated times. (H) Immunohistochemical staining of p-AKT in xenograft tissues (scale bar: 100 μm). (I) Immunoblot analysis of LC3 in cells transfected with empty vector or CA-AKT, following treatment with or without ECON (20 μmol/L, 24 h). (J) Immunofluorescence analysis of LC3 puncta treated as in (I), scale bar: 10 μm. (K) Heatmap of DEGs identified by RNA-seq. (L) Volcano Plots of DEGs in (K). (M) Immunohistochemical staining of ATF3 in xenograft tissues (scale bar: 100 μm). (N) Immunoblot and qPCR analysis of ATF3 in cells treated with indicated concentrations of ECON for 24 h. (O) Correlation analysis between ATF3 and p-AKT in xenograft tissues and public dataset. (P) Immunohistochemical staining of ATF3 in 65 PDAC patients. Correlation analysis of ATF3 and PDAC differentiation. (Q) Kaplan−Meier analysis of PDAC patients in (P). Data are presented as mean ± SD, $n = 3$; *$P < 0.05$; **$P < 0.01$, ***$P < 0.001$, ns, no significant.

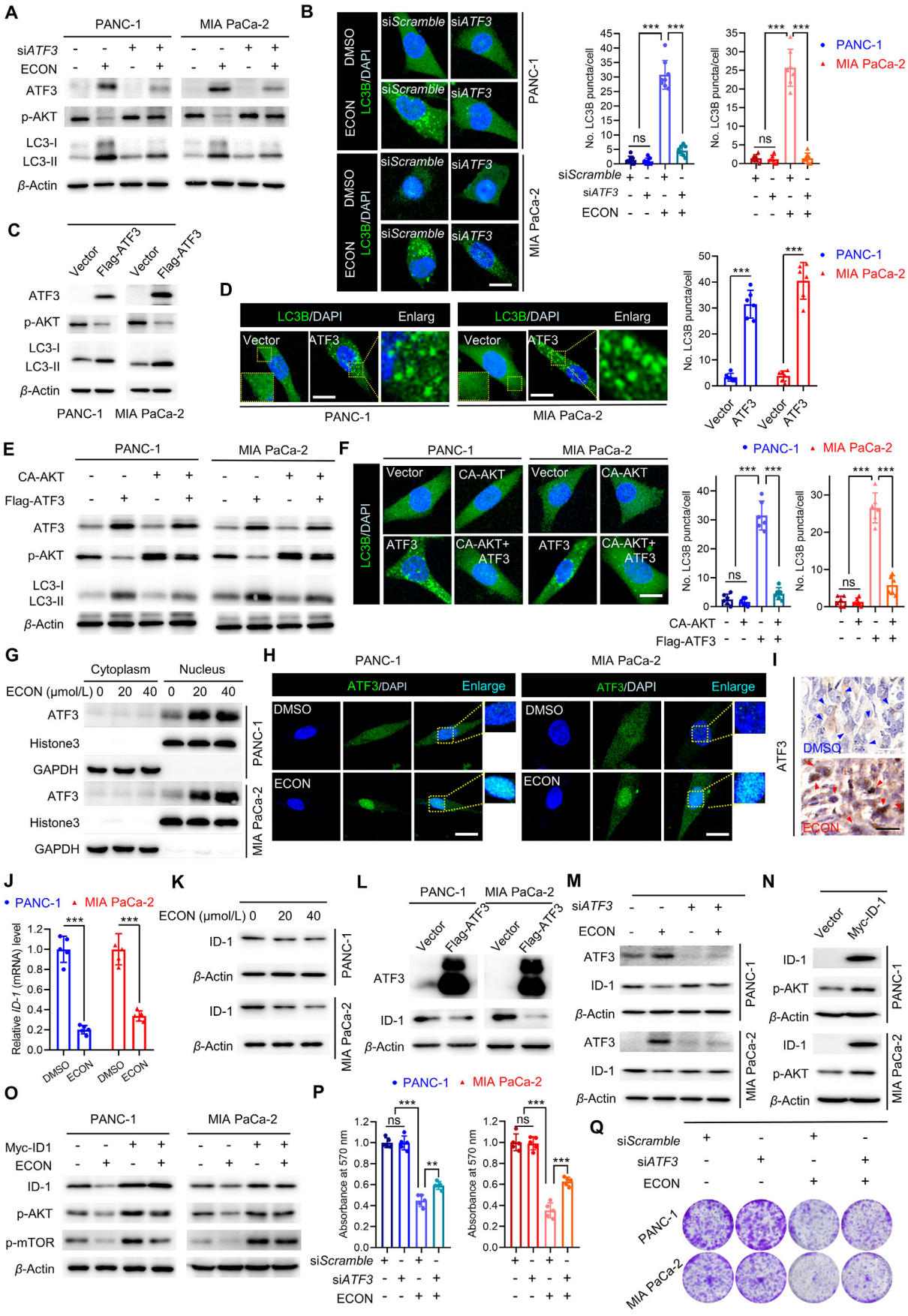
A
PANC-1
MIA PaCa-2
siATF3
ECON
ATF3
p-AKT
LC3-I
LC3-II
β-Actin
B
siScramble
siATF3
DMSO
ECON
LC3B/DAPI
PANC-1
MIA PaCa-2
No. LC3B puncta/cell
ns
C
Vector
Flag-ATF3
D
LC3B/DAPI
Enlarg
E
CA-AKT
Flag-ATF3
F
CA-AKT
CA-AKT+ ATF3
G
Cytoplasm
Nucleus
ECON (μmol/L) 0 20 40
Histone3
GAPDH
H
ATF3/DAPI
I
DMSO
ECON
J
Relative ID-1 (mRNA) level
K
ID-1
L
M
N
O
Myc-ID1
p-mTOR
P
Absorbance at 570 nm
Q

survival in TCGA and Oncomine datasets and found that a high level of ATF3 was correlated with improved cumulative survival (Fig. S5I and S5J). Moreover, we performed a retrospective analysis in 65 PDAC cases. Consistently, decreased ATF3 expression was correlated with poor differentiation and shorter overall survival in PDAC patients (Fig. 4P and Q). Next, we explored the potential mechanism underlying the ECON-induced upregulation of ATF3. Indeed, numerous studies have reported that azole antifungal drugs, including ECON, exhibit therapeutic effects by generating excessive intracellular reactive oxygen species (ROS)[28,29]. Furthermore, the accumulation of ROS has been linked to an enhanced translocation of NF-E2-related factor 2 (Nrf2) to the nucleus, where this transcription factor binds to the antioxidant response element sequences located in the promoter region of the *ATF3* gene, thereby promoting its transcription[30−32]. In line with these previous studies, we found that ECON treatment significantly upregulated the intracellular ROS levels of PDAC cells, accompanied by increased expression of Nrf2 in a dose-dependent manner (Supporting Information Fig. S6A and S6B). Moreover, the ECON-triggered transcriptional upregulation of *ATF3* was markedly compromised by small interfering RNA (siRNA)-mediated knockdown of *NFE2L2* (Fig. S6C and S6D), indicating the involvement of Nrf2 in regulating ATF3 expression, at least in the context of ECON exposure. Taken together, these data indicate that the ATF3/AKT axis is involved in ECON-induced autophagy and that ATF3 may serve as an indicator of improved prognosis.

### 3.5. *ECON inhibits PDAC cell growth by ATF3/ID-1/AKT-triggered autophagy*

Considering the involvement of the ATF3/AKT axis in ECON-induced autophagy, we next conducted loss- and gain-of-function studies to determine how ATF3 functions in this process. ECON failed to induce elevation of LC3-II levels and LC3 puncta accumulation in si*ATF3*-treated PDAC cells (Fig. 5A and B), while exogenous ATF3 expression led to higher levels of LC3-II expression and LC3 puncta accumulation (Fig. 5C and D), which could be attenuated by CA-AKT (Fig. 5E and F). These findings elucidate that the ATF3/AKT axis is required for ECON-induced autophagy. Given the crucial role of ATF3 as a TF in metabolic homeostasis[33], we next determined whether ATF3 functioned through transcriptional regulation with ECON treatment. As expected, PDAC cells exhibited increased nuclear expression of ATF3 in response to ECON (Fig. 5G), which was consistent with the results from immunofluorescence and IHC analysis (Fig. 5H and I). Since the engagement of ATF3 for ID-1 transcriptional repression[34], a key regulator in AKT signaling and a potential target for indicating poor prognosis in PDAC[35,36] (Supporting Information Fig. S7A−S7G), we assumed that ATF3 might elicit ECON-induced autophagy by downregulating the ID-1-mediated AKT pathway. As expected, we showed that ECON treatment decreased the *in vitro* production of ID-1 at both the mRNA and protein levels (Fig. 5J and K), mirroring the effect of exogenous ATF3 expression on PDAC cells (Fig. 5L). In contrast, this reduction in the expression of ID-1 could be largely prevented by genetic silencing of *ATF3* (Fig. 5M), indicating that ATF3 functions as a transcriptional repressor of ID-1 in PDAC cell lines. In addition, by gain- and loss-of-function studies of ID-1 in PDAC cells, we uncovered a positive regulatory relationship between ID-1 levels and the degree of AKT activation (p-AKT expression) (Fig. 5N, O, and Fig. S7H). These data imply that ECON negatively regulates the AKT pathway *via* the ATF3/ID-1 axis.

To further confirm the contribution of ATF3 to the cytotoxicity of ECON, we performed MTT and colony formation assays with or without *ATF3* silencing. ATF3 inhibition restored cell growth in ECON-treated PDAC cells (Fig. 5P, Q, and Fig. S7I). Taken together, these results indicate that ECON inhibits PDAC cell growth by ATF3/ID-1/AKT-triggered autophagy.

### 3.6. *Dysfunctional autophagy induced by ECON elicits ER stress-mediated apoptosis*

Considering that impaired autophagic flux could lead to endoplasmic reticulum (ER) stress, which further contributes to increased apoptotic cell death in cancers[37], we speculate that dysfunctional autophagy induced by ECON might elicit apoptosis mainly *via* ER stress. In view of the serious negative impact of ER stress on cell survival, we first determined the role of ER stress in ECON-mediated growth inhibition. Indeed, the expression of ER stress sensors (IRE1$\alpha$, PERK and CHOP) was upregulated with ECON treatment in a dose-dependent manner, and this upregulation could be counteracted by 4-phenylbutyrate (4-PBA, an ER stress inhibitor), which was found to attenuate the growth-inhibitory effect of ECON, supporting the contribution of ER stress to the anti-PDAC effect of ECON (Fig. 6A−D). We next investigated whether ER stress was actually attributed to ECON-triggered dysregulated autophagy. Notably, the upregulation of these sensors could be counteracted by genetic silencing of *ATG5* or *BECN1*. In contrast, silencing *IRE1α*, *PERK* and *BIP* (an ER molecular chaperone) had no obvious effect on LC3-II accumulation (Fig. 6E−H and Supporting Information Fig. S8A). Importantly, we noted that LC3II was increased before ER stress

**Figure 5** ECON inhibits PDAC cell growth by ATF3/ID-1/AKT-triggered autophagy. (A) Immunoblot analysis of ATF3, p-AKT and LC3 in PDAC cells transfected with si*Scramble*, si*ATF3*, followed by treatment with or without ECON (20 μmol/L, 24 h). (B) Immunofluorescence analysis of LC3 puncta treated as in (A), scale bar: 10 μm. (C) Immunoblot analysis of ATF3, p-AKT and LC3 in cells transfected with empty vector or Flag-ATF3 plasmid. (D) Immunofluorescence analysis of LC3 puncta treated as in (C), scale bar: 10 μm. (E) Immunoblot analysis of LC3, ATF3 and p-AKT levels in cells co-transfected with Flag-ATF3 and CA-AKT. (F) Immunofluorescence analysis of LC3 puncta in cells treated as in (E), scale bar: 10 μm. (G) Cytoplasmic and nuclear fractions of ATF3 were analyzed by immunoblot analysis. (H) Immunofluorescence analysis of ATF3 in cells treated with ECON (20 μmol/L, 24 h), scale bar: 10 μm. (I) Immunohistochemical staining of ATF3 in xenograft tissues (scale bar: 20 μm). (J, K) qPCR and immunoblot analysis of ID-1 in PDAC cells treated as in (H). (L) Immunoblot analysis of ATF3 and ID-1 in PDAC cells treated as in (C). (M) Immunoblot analysis of ATF3 and ID-1 in PDAC cells treated as in (A). (N) Immunoblot analysis of ID-1 and p-AKT in cells transfected with empty vector or Myc-ID-1 plasmid. (O) Immunoblot analysis of ID-1, p-AKT and p-mTOR in PDAC cells transfected with empty vector or Myc-ID-1 plasmid, followed by treatment with or without ECON (20 μmol/L, 24 h). (P, Q) MTT and colony formation of PDAC cells treated as in (A). Data are presented as mean ± SD, $n = 3$; $^{*}P < 0.05$; $^{**}P < 0.01$, $^{***}P < 0.001$, ns, no significant.

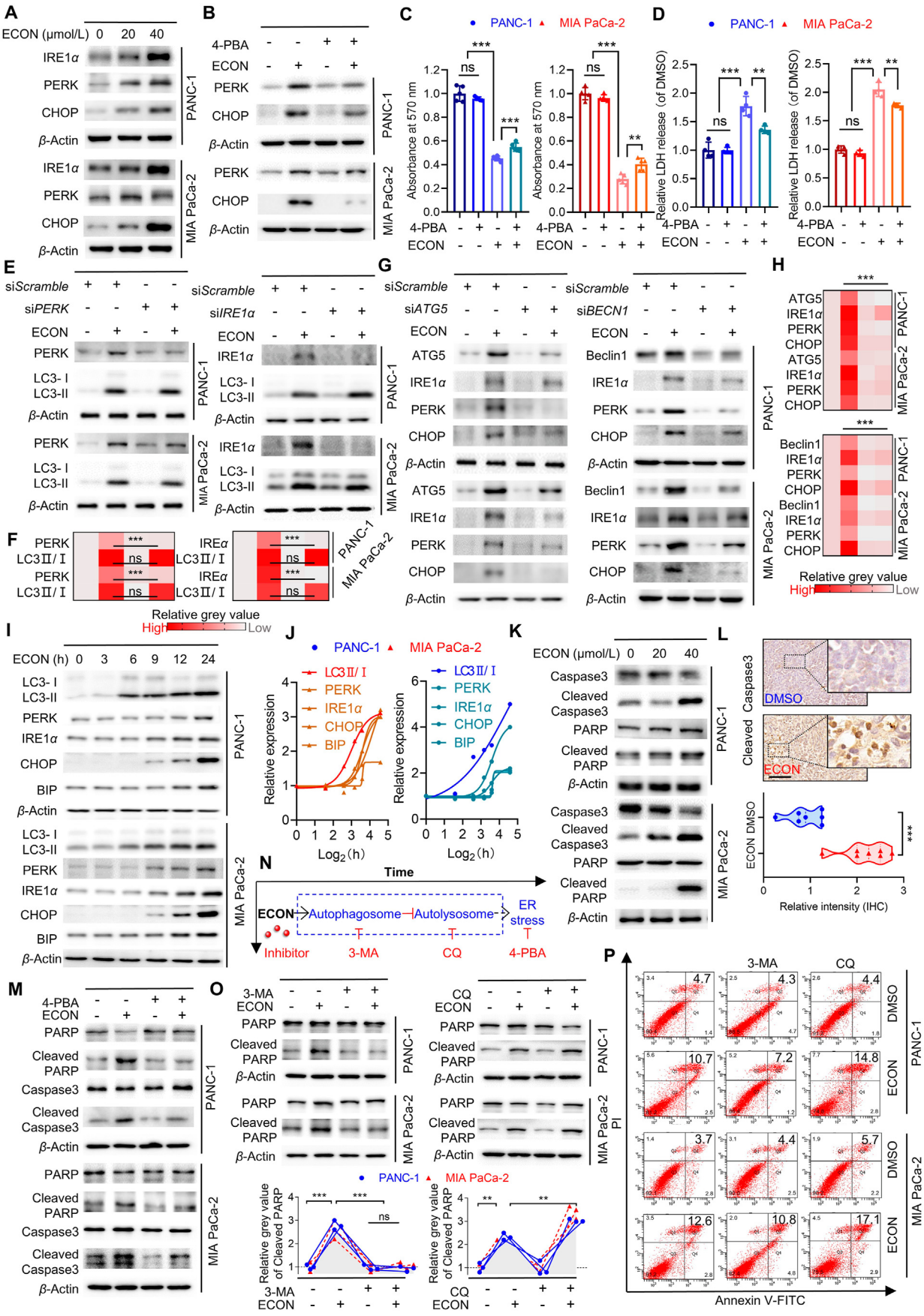
A
ECON (μmol/L) 0 20 40
IRE1α
PERK
CHOP
β-Actin
PANC-1
MIA PaCa-2
B
4-PBA
ECON
C
PANC-1 MIA PaCa-2
Absorbance at 570 nm
ns
D
Relative LDH release (of DMSO)
E
siScramble
siPERK
siIRE1α
LC3- I
LC3-II
F
PERK LC3Ⅱ/Ⅰ
IREα LC3Ⅱ/Ⅰ
Relative grey value
High
Low
G
siATG5
siBECN1
ATG5
Beclin1
H
I
ECON (h) 0 3 6 9 12 24
BIP
J
LC3Ⅱ/Ⅰ
PERK
IRE1α
CHOP
BIP
Relative expression
Log2(h)
K
ECON (μmol/L) 0 20 40
Caspase3
Cleaved Caspase3
PARP
Cleaved PARP
L
DMSO
ECON
Cleaved Caspase3
Relative intensity (IHC)
M
4-PBA
ECON
N
Time
ECON
Autophagosome
Autolysosome
ER stress
Inhibitor
3-MA
CQ
4-PBA
O
3-MA
CQ
Relative grey value of Cleaved PARP
P
3-MA
CQ
DMSO
ECON
PI
Annexin V-FITC
4.7
4.3
4.4
10.7
7.2
14.8
3.7
4.4
5.7
12.6
10.8
17.1

induction (Fig. 6I and J). Therefore, dysfunctional autophagy induced by ECON, as a prerequisite, is required for ER stress.

To further address whether ER stress inhibited PDAC cell growth by inducing apoptosis, we conducted immunoblot and immunohistochemical analyses and found that the expression of apoptosis markers was significantly elevated in response to ECON (Fig. 6K and L). This elevation could be attenuated by 3-MA or 4-PBA but reinforced by CQ treatment (Fig. 6M−O), echoing the results from flow cytometric analysis (Fig. 6P). Moreover, we evaluated the impact of apoptosis on cell growth. As depicted in Fig. S8B, an apoptosis inhibitor (z-VAD) alleviated the cytotoxicity of ECON in PDAC cells. These data demonstrate that dysfunctional autophagy induced by ECON elicits ER stress-mediated apoptosis.

### 3.7. *Synergistic action is obtained by combining ECON with trametinib*

Another issue to consider is that the dependence of PDAC in autophagy could be further strengthened during pharmacological inhibition of KRAS effectors, ERK or MEK, serving as a resistance-conferring mechanism exploited by PDAC cells[38,39]. Therefore, synchronized inhibition of MEK1/2 and autophagy, *i.e.*, trametinib/CQ combination therapy, exhibited synergistic effects against PDAC both *in vivo* and *in vitro*[38]. In this regard, to further determine whether a similar cytotoxicity could be also observable when combined with ECON (Fig. 7A), we verified the effects of trametinib on PDAC growth and autophagic flux firstly. Mirroring previous studies, trametinib decreased cell growth and boosted autophagic flux of PDAC cells in a dose-dependent manner (Fig. 7B and C). As expected, when trametinib was combined with low-dose, but not killing-dose, ECON, the cytotoxicity against PDAC cells was significantly enhanced compared to that of either inhibitor alone (Fig. 7D and Supporting Information Fig. S9A). As shown in Fig. 7C, we thus investigated whether trametinib-induced autophagic flux could be blocked by ECON, contributing to the synergistic anti-PDAC effect. Indeed, the growth-inhibitory activity caused by combinational therapy was partially alleviated after genetic silencing of *ATG5* or *BECN1* (Fig. 7E). Moreover, ECON augmented trametinib-triggered LC3-II accumulation while obstructing trametinib-induced p62 degradation (Fig. S9B), both of which demonstrated that trametinib-mediated protective autophagy could be hijacked by ECON for therapeutic purposes. In support of the results of cell line studies, this synergistic effect of ECON plus trametinib was further confirmed using PDAC PDOs (Fig. 7F). Finally, in addition to the PDO model, we compared the synergistic efficacy between trametinib/ECON and trametinib/HCQ combination by establishing a PANC-1 xenograft model and found that ECON, acting as a combination partner, exerted stronger trametinib-sensitizing effects on PDAC (Fig. 7G−I), hinting at its potential clinical prospects in combined pharmacotherapy.

## 4. Discussion

The 5-year survival rate of PDAC patients is still less than 10%[2], which is mainly attributed to its high metastatic rate at diagnosis, coupled with treatment failures, relapses and interruptions caused by *de novo* resistance or toxic side effects to current standard-of-care regimens[2,6]. Therefore, reagents designed to target KRAS or its effectors are expected to have better efficacy towards long-term survival in PDAC patients. Unfortunately, given the prevailing perception that RAS oncoproteins are undruggable with compensatory adjustment to agents targeting their downstream effectors, the expected outcome has failed to materialize[40,41]. Despite these challenges, certain progress has indeed been attained with sequential development in the search for selective $KRAS^{G12C}$ inhibitors[42,43]. Nevertheless, for these agents, the time frame from preclinical/clinical trials to clinical application is still a long way off. This is, in part, due to the notion that the adaptable nature of carcinoma cells tends to be far more powerful than previously realized[44].

This predicament has sparked growing interest in drug repurposing. Compared to *de novo* drug synthesis, this alternative strategy possesses significant advantages (lower investment costs, faster-paced development, etc.), supporting the concept that drug repurposing represents a promising approach to alleviating the situation[7]. Despite the high risks of retinopathy[45], treating PDAC with HCQ undoubtedly serves as an exemplary model. Inspired by HCQ and other successful instances of repurposing[11,12], the potential additional effects of anti-malarial/fungal/parasitic/viral agents warranted re-examination in PDAC. Fortunately, by judging therapeutic efficacy, ECON stands out among such compounds.

Actually, the prosurvival role of autophagy explains why autophagy inhibition becomes an effective therapeutic strategy against carcinomas, especially in PDAC. However, this explanation could hardly apply in certain contexts because it ignored its dual characteristics. For instance, cells undergoing apoptosis can be manipulated by autophagy towards opposite fates, *i.e.*, survival or apoptotic promotion[46]. Such seemingly paradoxical effects rely largely on what kind of substrates to be degraded by autophagy, recapitulating as a context-dependent process[46]. For ECON exposure, we clarified the relationship between ECON-induced autophagy and apoptosis in PDAC cells, thus providing a logical explanation for its potent therapeutic responses against PDAC.

**Figure 6** Dysfunctional autophagy induced by ECON elicits ER stress-mediated apoptosis. (A) Immunoblot analysis of IRE1α, PERK and CHOP in cells treated with indicated concentrations of ECON for 24 h. (B) Immunoblot analysis of PERK and CHOP in PDAC cells treated with or without ECON (20 μmol/L) in the presence or absence of 4-PBA (2 mmol/L, 24 h). (C, D) The MTT and LDH release assay of cells treated as in (B). (E, F) Immunoblot analysis of LC3 in cells transfected with si*Scramble*, si*PERK* or si*IRE1α*, followed by treatment with or without ECON (20 μmol/L, 24 h). (G, H) Immunoblot analysis of IRE1α, PERK and CHOP in cells transfected with si*Scramble*, si*ATG5* or si*BECN1*, followed by treatment with or without ECON (20 μmol/L, 24 h). (I, J) Immunoblot analysis of LC3, PERK, IRE1α, CHOP and BIP in cells treated with ECON (20 μmol/L) for indicated times. Schematic of molecular events occurring in PDAC cells in response to ECON. (K) Immunoblot analysis of PARP, cleaved PARP, caspase3 and cleaved caspase3 in cells treated as in (A). (L) Immunohistochemical staining of cleaved caspase3 in xenograft tissues (scale bar: 100 μm). (M) Immunoblot analysis of PARP, cleaved PARP, caspase3 and cleaved caspase3 in PDAC cells treated as in (B). (N, O) Immunoblotting analysis of PARP and cleaved PARP in cells treated with 3-MA (5 mmol/L) or CQ (10 μmol/L, 24 h). (P) Flow cytometric analysis of PDAC cells treated as in (N). Data are presented as mean ± SD, $n = 3$; $^{*}P < 0.05$; $^{**}P < 0.01$, $^{***}P < 0.001$, ns, no significant.

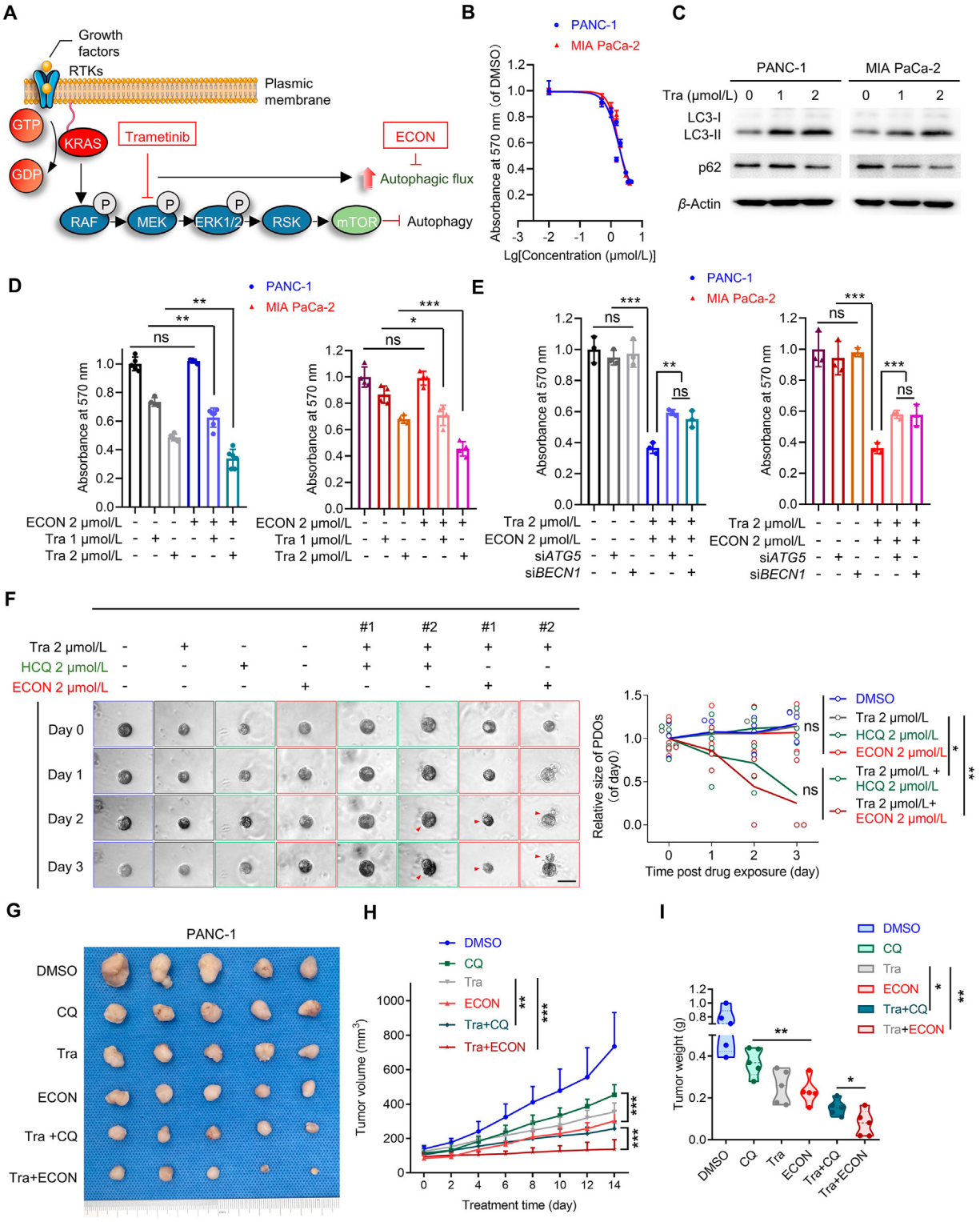


**Figure 7** Synergic action is obtained by combining ECON with trametinib. (A) Schematic overview. (B) MTT assay of PDAC cells incubated with trametinib for 48 h. (C) Immunoblot analysis of LC3 and p62 in cells treated with indicated concentrations of trametinib. (D) MTT assay of PDAC cells incubated with indicated concentrations of trametinib in the presence or absence of ECON (1 or 2 μmol/L). (E) MTT assay of PDAC cells incubated with or without combination of trametinib and ECON in the presence or absence of si*ATG5* and si*BECN1*. (F) Brightfield images of organoids treated as in (D), scale bar: 100 μm. (G–I) PANC-1 cells were injected subcutaneously into nude mice. When the tumor volumes reached ~100 $mm^3$, mice bearing PDAC xenografts were randomly divided into 6 groups and received following treatments, respectively, including i) vehicle; ii) 25 mg/kg ECON; iii) 25 mg/kg CQ; iv) 1 mg/kg trametinib; v) 25 mg/kg ECON + 1 mg/kg trametinib; vi) 25 mg/kg CQ + 1 mg/kg trametinib. Images (G), volumes measured at the indicated time points (H) and weights (I) of isolated tumors were shown. Data are presented as mean ± SD, $n = 3$; $^*P < 0.05$; $^{**}P < 0.01$, $^{***}P < 0.001$, ns, no significant.

Beyond that, with the emerging roles of autophagy in the acquisition of malignant behaviors of PDAC (*e.g.*, metastasis, resistance and immune evasion)[47−49], further investigation seems necessary to particularize the potential effect of ECON in these aspects.

Among those phenotypes, refractiveness to agents targeting downstream pathways of KRAS tends to be a representative example where autophagy serves as a resistance-conferring mechanism exploited by PDAC cells[38,39]. Specifically, MEK1/2 inhibition has been found to activate the LKB1/AMPK/ULK1 axis for autophagy induction[38]; in contrast, ERK inhibition could hijack metabolic processes for upregulating autophagy at multiple levels[39]. Fortuitously, enhanced therapeutic efficacy against PDAC has already been achieved by a combination of MEK/ERK inhibitor with HCQ/CQ in preclinical models[38,39]. In this manner, ECON could also increase the sensitivity to trametinib in PDAC cells by inducing autophagy arrest. Collectively, our study has demonstrated a potential role for ECON, which acts not only as a monotherapy agent but also as an alternative autophagy inhibitor combined with standard therapeutics in clinical practice, in achieving better outcomes in PDAC patients.

This antitumor effect of ECON against PDAC is in line with previous studies supporting similar impacts on several other types of cancers; however, there are certain instances where the involvement of a specific mechanism that leads to the induction of apoptosis has also been proposed[14,15,50]. Our data reveal that the cytotoxicity induced by ECON can mainly be attributed to the excessive accumulation of autophagosomes in PDAC cells, which results from the ATF3-mediated promotion of autophagy together with a decline in lysosomal biogenesis. Consequently, the accumulated autophagosomes give rise to the direct activation of ER stress-dependent apoptosis in PDAC cells, implying that the autophagic and apoptotic responses to ECON treatment may occur in a sequential manner. In addition, ECON is regarded as one of the most commonly used antifungal drugs, and its original target is cytochrome P450-dependent enzyme 14$\alpha$ demethylase (CYP51), which engages with the heme pocket[51,52]. More importantly, the expression of the CYP superfamily has been reported to be upregulated and associated with poor prognosis in different types of carcinomas[53−55]. Because of this, there is reason to believe that CYP51 may also be involved in the response of PDAC cells to ECON, and therefore, further investigations will be required to test this hypothesis in the future.

## 5. Conclusions

Guided by the strategy of drug repurposing, we have demonstrated that ECON, an antifungal compound, exhibits a potent therapeutic response against PDAC using patient-derived organoids, which tends to be an alternative to HCQ in terms of efficacy and safety. This cytotoxicity of ECON in PDAC cells depends on hijacking autophagy machinery, *i.e.*, decreased lysosomal biogenesis and excessive autophagy induction. The former results in attenuated autophagic flux, while the latter further contributes to the accumulation of autophagosomes, which is triggered by the ATF3/ID-1/AKT axis. In conclusion, our study provides direct preclinical and experimental evidence for the therapeutic efficacy of ECON in PDAC treatment and reveals a mechanism whereby ECON inhibits PDAC growth, laying the foundation for its potential therapeutic opportunity with translational significance in clinical practice.

## Acknowledgments

This work was funded by Guangdong Basic and Applied Basic Research Foundation (2019B030302012, China); National Key R&D Program of China (2020YFA0509400 and 2020YFC2002705); NSFC (81821002, 81790251 and 82130082, China); 1.3.5 project for disciplines of excellence, West China Hospital, Sichuan University (ZYJC21042, China).

## Author contributions

Canhua Huang and Qing Zhu designed and supervised the research. Ningna Weng, Siyuan Qin, Jiayang Liu, Jingwen Jiang, Li Zhou, Zhe Zhang, Ping Jin, Maochao Luo, Na Xie, and Liyuan Peng performed the experiments. Siyuan Qin and Kui Wang performed the bioinformatic analysis. Siyuan Qin and Xing Huang developed the animal and organoid models. Qing Zhu and Suxia Han provided the clinical samples. Siyuan Qin, Ajay Goel and Edouard C. Nice wrote the manuscript.

## Conflicts of interest

The authors declare no potential conflicts of interest.

## Appendix A. Supporting information

Supporting data to this article can be found online at https://doi.org/10.1016/j.apsb.2022.01.018.

## References

1. Kamisawa T, Wood LD, Itoi T, Takaori K. Pancreatic cancer. *Lancet* 2016;**388**:73−85.
2. Christenson ES, Jaffee E, Azad NS. Current and emerging therapies for patients with advanced pancreatic ductal adenocarcinoma: a bright future. *Lancet Oncol* 2020;**21**:e135−45.
3. Yang S, Wang X, Contino G, Liesa M, Sahin E, Ying H, et al. Pancreatic cancers require autophagy for tumor growth. *Genes Dev* 2011;**25**:717−29.
4. Rosenfeldt MT, O'Prey J, Morton JP, Nixon C, MacKay G, Mrowinska A, et al. p53 status determines the role of autophagy in pancreatic tumour development. *Nature* 2013;**504**:296−300.
5. Wolpin BM, Rubinson DA, Wang X, Chan JA, Cleary JM, Enzinger PC, et al. Phase II and pharmacodynamic study of autophagy inhibition using hydroxychloroquine in patients with metastatic pancreatic adenocarcinoma. *Oncol* 2014;**19**:637−8.
6. Adiseshaiah PP, Crist RM, Hook SS, McNeil SE. Nanomedicine strategies to overcome the pathophysiological barriers of pancreatic cancer. *Nat Rev Clin Oncol* 2016;**13**:750−65.
7. Pushpakom S, Iorio F, Eyers PA, Escott KJ, Hopper S, Wells A, et al. Drug repurposing: progress, challenges and recommendations. *Nat Rev Drug Discov* 2019;**18**:41−58.
8. Zhang Z, Zhou L, Xie N, Nice EC, Zhang T, Cui Y, et al. Overcoming cancer therapeutic bottleneck by drug repurposing. *Signal Transduct Target Ther* 2020;**5**:113.
9. Zhang Z, Zhang L, Zhou L, Lei Y, Zhang Y, Huang C. Redox signaling and unfolded protein response coordinate cell fate decisions under ER stress. *Redox Biol* 2019;**25**:101047.
10. Sullivan Jr DJ, Gluzman IY, Russell DG, Goldberg DE. On the molecular mechanism of chloroquine's antimalarial action. *Proc Natl Acad Sci U S A* 1996;**93**:11865−70.
11. Trachtenberg J, Pont A. Ketoconazole therapy for advanced prostate cancer. *Lancet* 1984;**2**:433−5.

12. Antonarakis ES, Heath EI, Smith DC, Rathkopf D, Blackford AL, Danila DC, et al. Repurposing itraconazole as a treatment for advanced prostate cancer: a noncomparative randomized phase II trial in men with metastatic castration-resistant prostate cancer. *Oncol* 2013;**18**:163−73.
13. Fromtling RA. Overview of medically important antifungal azole derivatives. *Clin Microbiol Rev* 1988;**1**:187−217.
14. Sobecks R, McCormick TS, Distelhorst CW. Imidazole antifungals miconazole and econazole induce apoptosis in mouse lymphoma and human T cell leukemia cells: regulation by Bcl-2 and potential role of calcium. *Cell Death Differ* 1996;**3**:331−7.
15. Choi EK, Park EJ, Phan TT, Kim HD, Hoe KL, Kim DU. Econazole induces p53-dependent apoptosis and decreases metastasis ability in gastric cancer cells. *Biomol Ther (Seoul)* 2020;**28**:370−9.
16. Boj SF, Hwang CI, Baker LA, Chio II , Engle DD, Corbo V, et al. Organoid models of human and mouse ductal pancreatic cancer. *Cell* 2015;**160**:324−38.
17. Tiriac H, Belleau P, Engle DD, Plenker D, Deschênes A, Somerville TDD, et al. Organoid profiling identifies common responders to chemotherapy in pancreatic cancer. *Cancer Discov* 2018;**8**:1112−29.
18. Zhou L, Gao W, Wang K, Huang Z, Zhang L, Zhang Z, et al. Brefeldin A inhibits colorectal cancer growth by triggering Bip/Akt-regulated autophagy. *FASEB J* 2019;**33**:5520−34.
19. Drost J, Clevers H. Organoids in cancer research. *Nat Rev Cancer* 2018;**18**:407−18.
20. Pattingre S, Tassa A, Qu X, Garuti R, Liang XH, Mizushima N, et al. Bcl-2 antiapoptotic proteins inhibit Beclin 1-dependent autophagy. *Cell* 2005;**122**:927−39.
21. Green DR, Levine B. To be or not to be? How selective autophagy and cell death govern cell fate. *Cell* 2014;**157**:65−75.
22. Perera RM, Stoykova S, Nicolay BN, Ross KN, Fitamant J, Boukhali M, et al. Transcriptional control of autophagy-lysosome function drives pancreatic cancer metabolism. *Nature* 2015;**524**:361−5.
23. Settembre C, Di Malta C, Polito VA, Garcia Arencibia M, Vetrini F, Erdin S, et al. TFEB links autophagy to lysosomal biogenesis. *Science* 2011;**332**:1429−33.
24. Han H, Cho JW, Lee S, Yun A, Kim H, Bae D, et al. TRRUST v2: an expanded reference database of human and mouse transcriptional regulatory interactions. *Nucleic Acids Res* 2018;**46**:D380−6.
25. Wang Z, Xu D, Ding HF, Kim J, Zhang J, Hai T, et al. Loss of ATF3 promotes Akt activation and prostate cancer development in a *Pten* knockout mouse model. *Oncogene* 2015;**34**:4975−84.
26. Chen C, Ge C, Liu Z, Li L, Zhao F, Tian H, et al. ATF3 inhibits the tumorigenesis and progression of hepatocellular carcinoma cells *via* upregulation of CYR61 expression. *J Exp Clin Cancer Res* 2018;**37**:263.
27. Hackl C, Lang SA, Moser C, Mori A, Fichtner-Feigl S, Hellerbrand C, et al. Activating transcription factor-3 (ATF3) functions as a tumor suppressor in colon cancer and is up-regulated upon heat-shock protein 90 (Hsp90) inhibition. *BMC Cancer* 2010;**10**:668.
28. Yu Y, Niapour M, Zhang Y, Berger SA. Mitochondrial regulation by c-Myc and hypoxia-inducible factor-1 alpha controls sensitivity to econazole. *Mol Cancer Ther* 2008;**7**:483−91.
29. Tits J, Berman J, Cammue BPA, Thevissen K. Combining miconazole and domiphen bromide results in excess of reactive oxygen species and killing of biofilm cells. *Front Cell Dev Biol* 2020;**8**:617214.
30. Dziunycz PJ, Lefort K, Wu X, Freiberger SN, Neu J, Djerbi N, et al. The oncogene ATF3 is potentiated by cyclosporine A and ultraviolet light A. *J Invest Dermatol* 2014;**134**:1998−2004.
31. Kim KH, Jeong JY, Surh YJ, Kim KW. Expression of stress-response ATF3 is mediated by Nrf2 in astrocytes. *Nucleic Acids Res* 2010;**38**:48−59.
32. Kha ML, Hesse L, Deisinger F, Sipos B, Röcken C, Arlt A, et al. The antioxidant transcription factor Nrf2 modulates the stress response and phenotype of malignant as well as premalignant pancreatic ductal epithelial cells by inducing expression of the ATF3 splicing variant ΔZip2. *Oncogene* 2019;**38**:1461−76.
33. Ku HC, Cheng CF. Master regulator activating transcription factor 3 (ATF3) in metabolic homeostasis and cancer. *Front Endocrinol (Lausanne)* 2020;**11**:556.
34. Kang Y, Chen CR, Massagué J. A self-enabling TGFbeta response coupled to stress signaling: smad engages stress response factor ATF3 for Id1 repression in epithelial cells. *Mol Cell* 2003;**11**:915−26.
35. Wang L, Man N, Sun XJ, Tan Y, García-Cao M, Liu F, et al. Regulation of AKT signaling by Id1 controls t(8;21) leukemia initiation and progression. *Blood* 2015;**126**:640−50.
36. Huang YH, Hu J, Chen F, Lecomte N, Basnet H, David CJ, et al. ID1 mediates escape from TGF$\beta$ tumor suppression in pancreatic cancer. *Cancer Discov* 2020;**10**:142−57.
37. Senft D, Ronai ZA. UPR, autophagy, and mitochondria crosstalk underlies the ER stress response. *Trends Biochem Sci* 2015;**40**:141−8.
38. Kinsey CG, Camolotto SA, Boespflug AM, Guillen KP, Foth M, Truong A, et al. Protective autophagy elicited by RAF→MEK→ERK inhibition suggests a treatment strategy for RAS-driven cancers. *Nat Med* 2019;**25**:620−7.
39. Bryant KL, Stalnecker CA, Zeitouni D, Klomp JE, Peng S, Tikunov AP, et al. Combination of ERK and autophagy inhibition as a treatment approach for pancreatic cancer. *Nat Med* 2019;**25**:628−40.
40. Cox AD, Fesik SW, Kimmelman AC, Luo J, Der CJ. Drugging the undruggable RAS: mission possible?. *Nat Rev Drug Discov* 2014;**13**:828−51.
41. Drosten M, Barbacid M. Targeting the MAPK pathway in KRAS-driven tumors. *Cancer Cell* 2020;**37**:543−50.
42. Janes MR, Zhang J, Li LS, Hansen R, Peters U, Guo X, et al. Targeting KRAS mutant cancers with a covalent G12C-specific inhibitor. *Cell* 2018;**172**:578−589.e17.
43. Lanman BA, Allen JR, Allen JG, Amegadzie AK, Ashton KS, Booker SK, et al. Discovery of a covalent inhibitor of KRAS(G12C) (AMG 510) for the treatment of solid tumors. *J Med Chem* 2020;**63**:52−65.
44. Qin S, Jiang J, Lu Y, Nice EC, Huang C, Zhang J, et al. Emerging role of tumor cell plasticity in modifying therapeutic response. *Signal Transduct Target Ther* 2020;**5**:228.
45. Leung LS, Neal JW, Wakelee HA, Sequist LV, Marmor MF. Rapid onset of retinal toxicity from high-dose hydroxychloroquine given for cancer therapy. *Am J Ophthalmol* 2015;**160**:799−805.e1.
46. Levy JMM, Towers CG, Thorburn A. Targeting autophagy in cancer. *Nat Rev Cancer* 2017;**17**:528−42.
47. Görgülü K, Diakopoulos KN, Ai J, Schoeps B, Kabacaoglu D, Karpathaki AF, et al. Levels of the autophagy-related 5 protein affect progression and metastasis of pancreatic tumors in mice. *Gastroenterology* 2019;**156**:203−217.e20.
48. Wang F, Xia X, Yang C, Shen J, Mai J, Kim HC, et al. *SMAD4* gene mutation renders pancreatic cancer resistance to radiotherapy through promotion of autophagy. *Clin Cancer Res* 2018;**24**:3176−85.
49. Yamamoto K, Venida A, Yano J, Biancur DE, Kakiuchi M, Gupta S, et al. Autophagy promotes immune evasion of pancreatic cancer by degrading MHC-I. *Nature* 2020;**581**:100−5.
50. Dong C, Yang R, Li H, Ke K, Luo C, Yang F, et al. Econazole nitrate inhibits PI3K activity and promotes apoptosis in lung cancer cells. *Sci Rep* 2017;**7**:17987.
51. Zhang J, Li L, Lv Q, Yan L, Wang Y, Jiang Y. The fungal CYP51s: their functions, structures, related drug resistance, and inhibitors. *Front Microbiol* 2019;**10**:691.
52. Lamb DC, Kelly DE, Baldwin BC, Gozzo F, Boscott P, Richards WG, et al. Differential inhibition of *Candida albicans* CYP51 with azole antifungal stereoisomers. *FEMS Microbiol Lett* 1997;**149**:25−30.
53. Patel V, Liaw B, Oh W. The role of ketoconazole in current prostate cancer care. *Nat Rev Urol* 2018;**15**:643−51.
54. Pozzi A, Popescu V, Yang S, Mei S, Shi M, Puolitaival SM, et al. The anti-tumorigenic properties of peroxisomal proliferator-activated receptor alpha are arachidonic acid epoxygenase-mediated. *J Biol Chem* 2010;**285**:12840−50.
55. McFadyen MC, Melvin WT, Murray GI. Cytochrome P450 CYP1B1 activity in renal cell carcinoma. *Br J Cancer* 2004;**91**:966−71.